



TAMPEREEN TEKNILLINEN YLIOPISTO
TAMPERE UNIVERSITY OF TECHNOLOGY

MARIO CALVO HERNANDO
ELECTRONIC INSTRUMENTATION FOR A 3D ELECTRICAL IMPEDANCE
TOMOGRAPHY APPLICATION

Master of Science Thesis

Master of Science Thesis

Examiners: Professor Jari Hyttinen, and
postdoctoral researcher Edite Areias
Figueiras.

Examiners and topic approved in the
Faculty of Computing and Electrical
Engineering council meeting on March
4th 2015

ABSTRACT

Master Degree in Industrial Engineering

CALVO HERNANDO, MARIO: ELECTRONIC INSTRUMENTATION FOR A 3D ELECTRICAL IMPEDANCE TOMOGRAPHY APPLICATION

Master of Science Thesis, 49 pages, 3 Appendix pages

May 2015

Major: Industrial Engineering

Examiner: Professor Jari Hyttinen, and postdoctoral researcher Edite Areias Figueiras

Keywords: Bioimpedance, Electrical Impedance Spectroscopy, Electrical Impedance Tomography, Electronic Instrumentation

The thesis aims to present the electronic instrumentation required for an EIT application which aims to make an imaging reconstruction of living cells covered with blank hydrogel. Thus the accuracy of the impedance measurement along the frequency range will have a great importance.

The experiments performed are made for a 2D EIT system which allows us to extract useful information for the development of the future 3D system.

The thesis is divided into four parts: a theoretical study about the bioimpedance and the EIT, the measurement setup used during the course of the thesis and the possible alternatives, the presentation of the results obtained, discussion of results and the conclusion of the thesis.

The HF2IS Impedance Spectroscopy (Zurich Instruments AG, Switzerland) is the measurement equipment used to perform four-terminal impedance measurements. The spectroscopy is located in the laboratory of the BioMediTech Group at FinMedi. A multiplexing system has been designed, consisting of four 16x1 channels multiplexers which will be controlled by the digital outputs of the spectroscopy.

Besides, the electronic instrumentation required for the EIT system without the HF2IS spectroscope is presented as an aid to future stages of the project.

PREFACE

This thesis presents a research about the electronic instrumentation used for a 3D Electrical Impedance Tomography application based on the needs of the Human Spare Parts (HSP) project at the Institute of Biosciences and Medical Technology, BioMediTech of the Tampere University of Technology. The work was performed at FinnMedi building in the Tampere University of Technology area and inside the Department of Electronics and Communications Engineering.

Professor Jari Hyttinen and the postdoctoral researcher Edite Areias Figueiras are the supervisors of this thesis. Jari is the originator of most grand ideas and has managed the evolving of the whole project. Edite leads the project group in which this work is a part of the HSP project. Moreover, this thesis is a support for the research of the PhD student Mari Lehti-Polojärvi, whose work is focused on EIT applied to stem cells in hydrogel scaffold. The postdoctoral researcher Ana Soto de la Cruz has provided the hydrogel.

I would like to thank for this exchange experience to my home university, Universidad del País Vasco, and last but not least, to my family for encouraging me to go to Finland on an exchange from the first moment.

In Tampere, Finland, on 19th May 2015

Mario Calvo Hernando

TABLE OF CONTENTS

1. INTRODUCTION.....	1
2. BACKGROUND.....	2
2.1 Impedance	2
2.2 Parasitics of the R, C and L components.....	3
2.3 Ideal, real, and measured impedance values	3
2.4 Frequency dependency of the components.....	5
2.5 Four-Terminal Measurement.....	6
2.6 Bioimpedance	7
2.7 Electrical Impedance Tomography	13
2.7.1 EIT System Architecture	14
2.7.2 Frequency range	14
2.7.3 Error sources.....	15
2.8 Data Collection Strategy	16
2.8.1 Neighbouring Method	16
2.8.2 Opposite Method	17
2.8.3. Cross Method	17
2.8.4 Adaptive Method.....	18
3. EIT INSTRUMENTATION	20
3.1 Measurement Setup	20
3.1.1 Impedance Spectroscope	20
3.1.2 Multiplexing system	22
3.1.3 Software: ziControl & LabView.....	26
3.1.4 Electrode location.....	26
3.2 Alternative measurement setup.....	28
3.2.1 Constant current injector	28
3.2.2 Multiplexers.....	31
3.2.3 Cable shielding.....	32
3.2.4 Data acquisition System	33
4 RESULTS.....	35
4.1 R-C circuits and evaluation of the measurement setup	35

4.2	Hydrogel tests	37
4.3	Carrot tests	38
5.	DISCUSSION.....	42
5.1	Analysis of the measurement setup	42
5.2	Analysis of the results	43
5.3	Future work.....	44
6.	CONCLUSION	45
	REFERENCES.....	47
	APPENDIX A: COMPARISON TABLE OF MUX AND NO MUX	
	APPENDIX B: COMPARISON TABLE BETWEEN CHANNELS	
	APPENDIX C: LABVIEW PANEL CONTROL	

SYMBOLS AND ABBREVIATIONS

AC	Alternating current
CMC	Capacitive of the Cell Membrane
CMR	Resistance of the Cell Membrane
DAS	Data Acquisition System
DC	Direct current
DDS	Direct Digital Synthesizer
EIT	Electrical Impedance Tomography
GG	Gellam Gum
HF2IS	High Frequency Series 2 Impedance Spectroscopy
IA	Instrumentation Amplifier
I/O	Inputs/Outputs
MUX	Multiplexing
PLA	Polylactic acid
SRF	Self-Resonant Frequency
VCCS	Voltage Controlled Current Source
\varnothing	Diameter (mm)
ϵ_0	Permittivity (F/m)
ϵ_r	Complex Permittivity (F/m)
ϵ_∞	Permittivity at high frequency (F/m)
ϵ_s	Permittivity at low frequency (F/m)
σ	Conductivity ($\Omega \cdot m$)
ω	Angular frequency (rad/s)
τ	Relaxing time
2D	Two dimensional
3D	Three dimensional
A	Surface area of the parallel plates
C_0/C_i	Stray capacitance of the cables and switchers
d	Distance between the plates
f_c	Relaxation frequency
K	Dielectric Constant
R_∞	Resistivity at high frequency (Ω)
R_s	Resistivity at low frequency (Ω)
R_i	Intracellular Resistance
R_e	Extracellular Resistance
V_{CM}	Common Mode Voltage
X_C	Capacitive Reactance (Ω)
X_L	Inductive Reactance (Ω)

1. INTRODUCTION

As it is known, every biological sample or tissue has the dielectric property to produce an opposition against an alternating current flow, as well called bioimpedance. Due to this property, it is possible to distinguish unequivocally between two tissues, cells or organs with a simple impedance measurement. The Electrical Impedance Tomography (EIT) is a non-invasive technique which uses this property to make the image reconstruction.

The mentioned technique is valuable in the researching of tissue engineering and regenerative medicine, as it allows us to analyse the biological cells with no damage due to the low electrical current used.

There is a direct relation between the size and shape of the cell, and the measured impedance value at low frequencies. On the other hand, at high frequencies we can obtain information about the internal composition of the cell due to the cytoplasmic resistance. Therefore, it is essential to study the bioimpedance properties and its equivalent electrical models.

For measuring the impedance of those cells, tissues or organs along a frequency range, it is required to use accurate electronic instrumentation. This electronic setup has to provide a constant current flow and a voltage measurement (four-terminal measurement), information required by the imaging reconstruction algorithms. Yet, at the same time, there are many EIT architectures. In this case, the system will be based on a single current injector and a single voltage measurement module, with a multiplexing system in between them, and the electrodes.

For the four-terminal measurement, the chosen option is the HF2IS Impedance Spectroscopy (Zurich Instruments AG, Switzerland), located in the laboratory of the BioMediTech Group at FinMedi, Tampere. The multiplexing system consists of four 16x1 channels multiplexers which will be controlled by the digital outputs of the spectroscopy through the Digital I/O breakout board (Zurich Instruments AG, Switzerland).

Control system was implemented in LabView program provided by Zurich instruments (see Appendix C), which will allow to automate the impedance tomography process considering the electrode topology and data collection strategy, the variable range of frequency and the speed of multiplexing.

Finally, several tests are performed over different samples as R-C circuits, hydrogel and biological samples (carrot).

2. BACKGROUND

The EIT is a technique based on the electrical impedance measurement as its name suggests, thus this chapter introduces the principles of the impedance, the bioimpedance and the EIT systems.

2.1 Impedance

The impedance is generally defined as the total opposition a device or circuit offers to the flow of an AC at a given frequency, and is represented as a complex quantity which is graphically shown on a vector plane, figure 2.1. Impedance is an important parameter used to characterize electronic circuits, components, and the materials used to make components.

An impedance vector consists of a real part, R , and an imaginary part, X . Impedance can be expressed using the rectangular-coordinate form, $R + jX$, or in the polar form as a magnitude and phase angle: $|Z| \angle \theta$. Figure 2.1 also shows the mathematical relationship between R , X , $|Z|$, and θ . In some cases, using the reciprocal of impedance is mathematically expedient. Impedance is a commonly used parameter and is especially useful for representing a series connection of resistance and reactance, because it can be expressed simply as a sum, R and X .

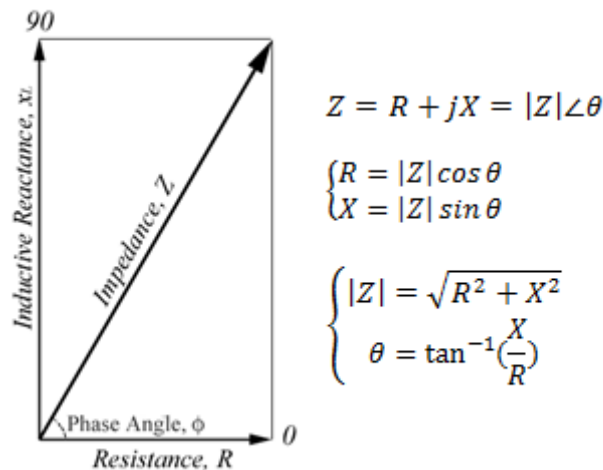


Figure 2.1 Impedance vector

Reactance takes two forms: X_L and capacitive X_C . By definition, $X_L = 2\pi fL$ and $X_C = 1/(2\pi fC)$, where the frequency of interest is f , L is inductance, and C is capacitance. $2\pi f$ can be substituted for by the angular frequency, ω , to represent $X_L = \omega L$ and $X_C = 1/(\omega C)$.

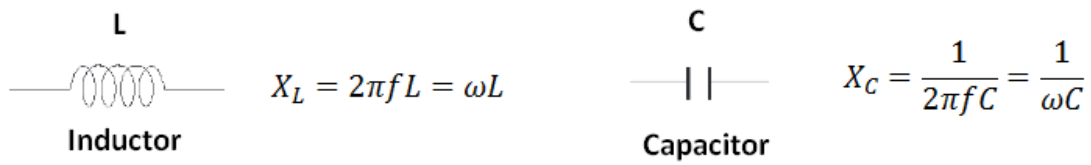


Figure 2.2 Reactance forms

2.2 Parasitics of the R, C and L components

As it is explained in the chapter 2.6, the bioimpedance can be represented by electrical models, thus the study of their components is essential to understand the impedance values obtained during the tests performed in this thesis. Besides, the parasitics of the electrical components will appear in the electronic instrumentation required in the EIT system as well.

The principal attributes of L, C, and R components are generally represented by the nominal values of capacitance, inductance, or resistance at specified or standardized conditions. However, all circuit components are neither purely resistive, nor purely reactive. They involve both of these impedance elements. This means that all real-world devices have parasitics, undesirable inductance in resistors, undesirable resistance in capacitors unwanted capacitance in inductors, etc. Different materials and manufacturing technologies produce varying amounts of parasitics [1]. In fact, many parasitics reside in components; therefore their selection will play a significant role in the electronic instrumentation.

2.3 Ideal, real, and measured impedance values

Every circuit component has an impedance parameter value but it is important to thoroughly understand what the value indicates in reality. The parasitics of the component and the measurement error sources, such as the electrode contact impedance and the Common Mode Voltage error in EIT, affect the value of impedance. Conceptually, there are three sorts of values: ideal, real and measured. These values are fundamental to understand the impedance value obtained and the possible reasons why the value measured sometimes does not correspond to the expected.

- The **ideal value** is the value of a circuit component that excludes the effects of its parasitics. The model of an ideal component assumes a purely resistive or reactive element that has no frequency dependence. In many cases, the ideal

value can be defined by a mathematical relationship involving the component's physical composition, e.g. $C = K\epsilon_0 \frac{A}{d}$. In the real world, ideal values are only of academic interest.

- The **real value** takes into consideration the effects of a component's parasitics, as it is represented in the figure 2.3 for a real-world capacitor. The real value represents effective impedance. The real value is the algebraic sum of the circuit component's resistive and reactive vectors, which come from the principal element and the parasitics. Since the parasitics yield a different impedance vector for a different frequency, the real value is frequency dependent [1]. This is something to keep in mind, especially for tomography, where the frequencies are normally higher than 100 kHz.

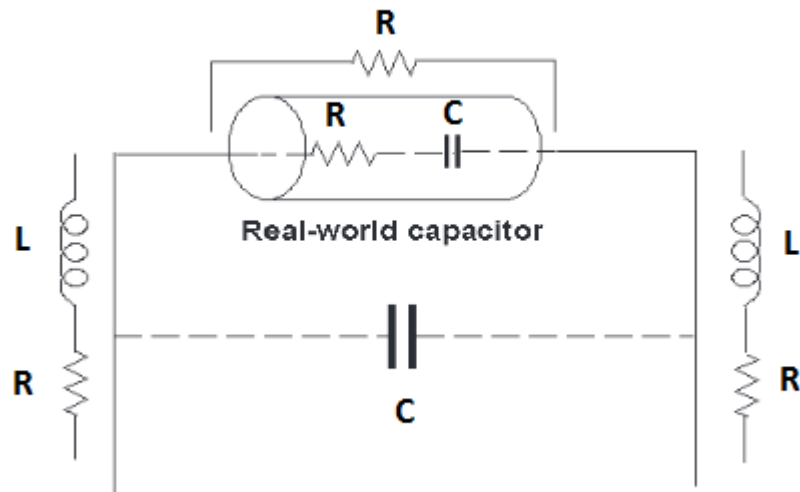


Figure 2.3 *Electrical model of a real-world capacitor* [1]

- The **measured value** is the value obtained from the measurement instrument; it reflects the instrument's inherent residuals and inaccuracies; see figure 2.4. Measured values always contain errors when compared to real values. They also vary intrinsically from one measurement to another; their differences depend on a multitude of considerations in regard to measurement uncertainties. The quality of measurements can be determined by comparing the measured value with the real value under certain conditions. The measured value is what is looked for, and the goal of measurement is to have the measured value be as close as possible to the real value.

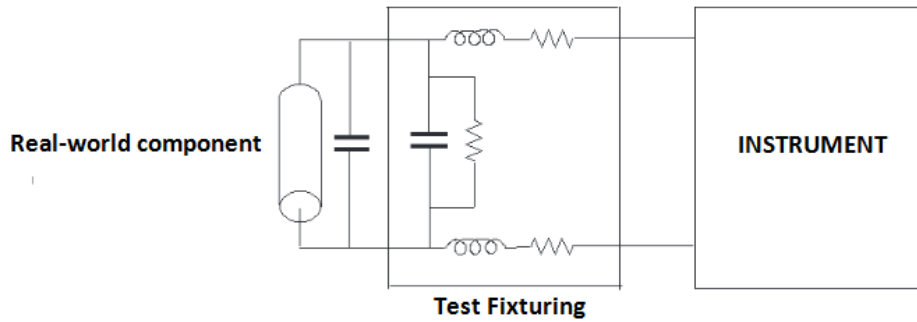


Figure 2.4 Electrical model of the measuring system [1]

2.4 Frequency dependency of the components

The test frequency will determine greatly the value obtain in the measurement.. Frequency dependency is common to all real-world components because of the existence of parasitics. Not all parasitics affect the measurement, but some prominent parasitics determine the component's frequency characteristics. The prominent parasitics will vary with the impedance value of the primary element. Figures 2.5 and 2.6 show the typical frequency response for real-world capacitors, inductors, and resistors. This analysis will be useful to understand the results obtained during our measurements and the error sources involved.

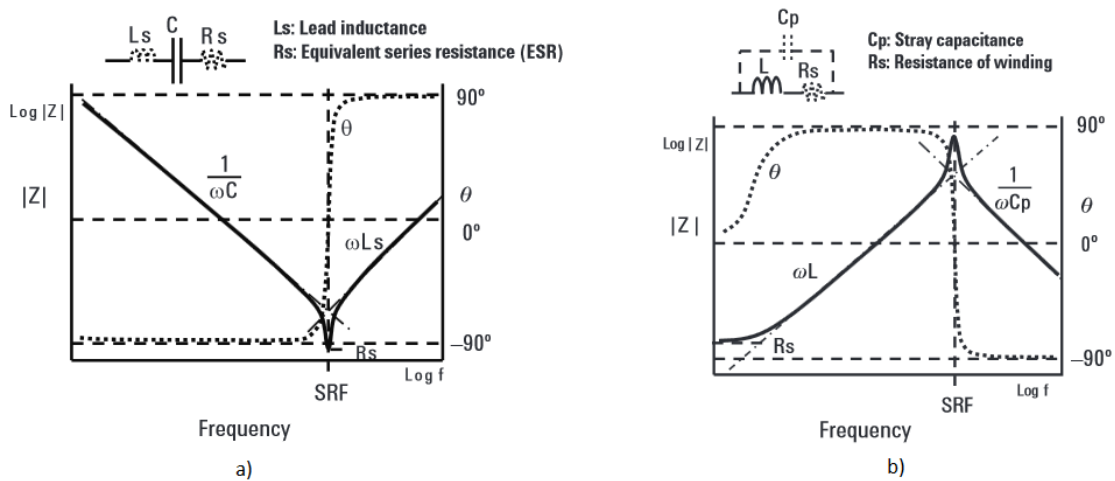


Figure 2.5 a) Frequency response of a general capacitor
b) Frequency response of a general inductor [1]

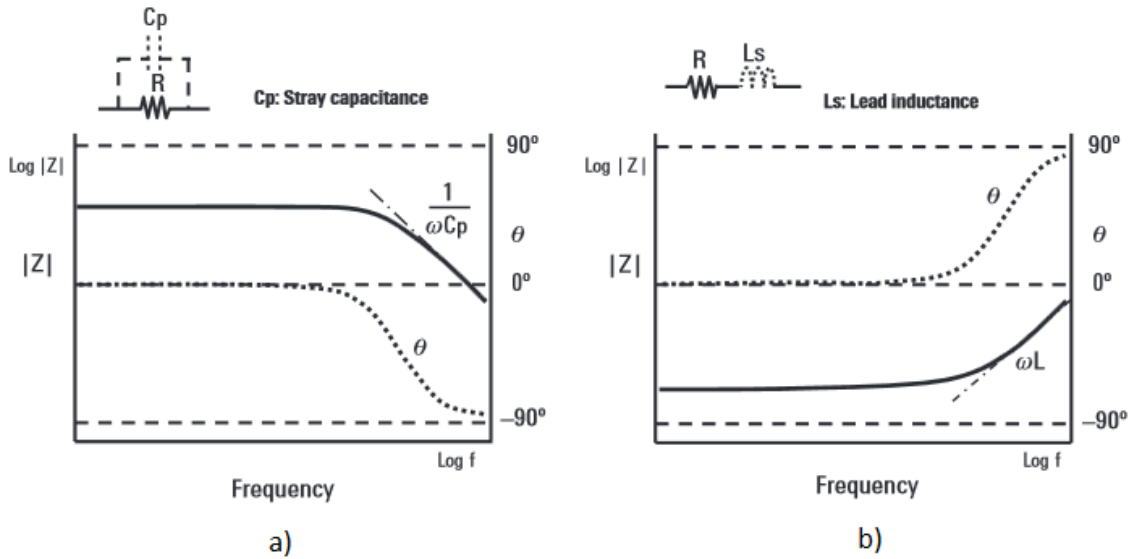


Figure 2.6 a) Frequency response of a high value resistor
 b) Frequency response of a low value resistor [1]

2.5 Four-Terminal Measurement

This technique consists on injecting a current through two electrodes and measuring the voltage from another two. Most of the EIT systems are based on it.

It reduces the effects of lead impedances and contact resistances because the signal current path and the voltage sensing leads are independent, as shown in the figure 2.6. The voltage sensing leads do not detect the voltage drop caused by the R_L , L_L , and R_C on the current leads. The impedances on the voltage sensing leads do not affect measurement because signal current scarcely flows through these leads.

Measurement errors due to the lead impedances and contact resistances are thereby eliminated. Accuracy for the lower impedance measurement range is thus improved typically down to $10 \text{ m}\Omega$ [1]. Measurement accuracy on the higher impedance range is not improved because the stray capacitances between the leads still remain.

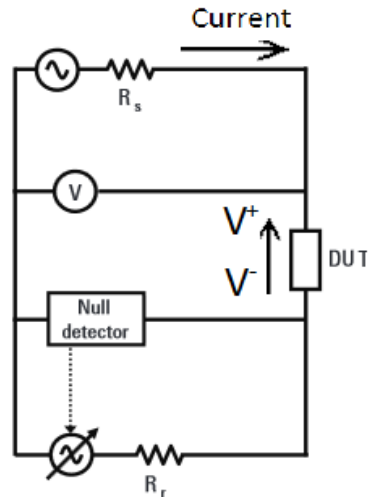


Figure 2.6 Four-terminal measurement configuration [1]

The figure 2.7 shows an idealization of a general four terminal measurement in a EIT system.

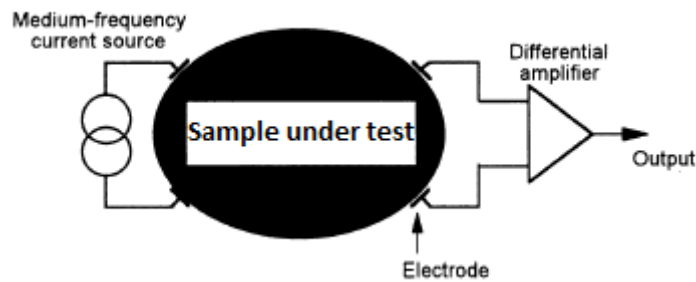


Figure 2.7 Impedance measurement in EIT [2]

2.6 Bioimpedance

First of all, before trying to measure anything, it is important to know the properties of the samples under test. Equivalent models of the cells will be really useful for the analysis.

Living organisms are composed of cells. Therefore, we define cells as the fundamental unit of life. Most cells are joined together by an extracellular matrix or by direct adhesion of a cell with another forming various joints. These cell groups result in tissues. The main component of the cells is the cell membrane whose structure is based on a lipid bilayer in which the proteins are distributed, allowing the formation of channels for ion exchange with the outside, figure 2.9.

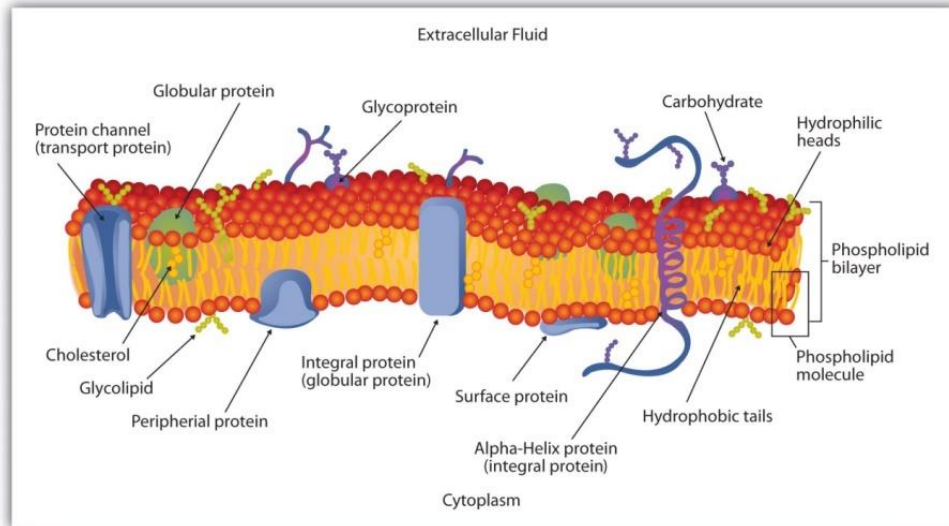


Figure 2.9 Schematic Diagram of a Cell Membrane [3]

Because of their internal configuration, the cell membrane acts as a dielectric interface and it can be considered as two plates of a capacitor. Therefore, when a constant electric field is applied, electrically charged ions move and accumulate on both sides of the membrane. However, when this electric field is alternating, with the frequency increasing, displacement currents appear through the cell wall, producing a relaxation phenomenon. This dielectric relaxation phenomenon is the result of several polarization dipoles and the charges movement which induces a phenomenon driving [4]. The charge carriers are primarily ions and the main source of the dipoles are the polar water molecules in tissue.

When the applied current frequency increases, the conductivity of most of the tissues raises from a low value, for direct current, which depends on the extracellular volume, to a constant level in the frequency range from 10 to 100 MHz.

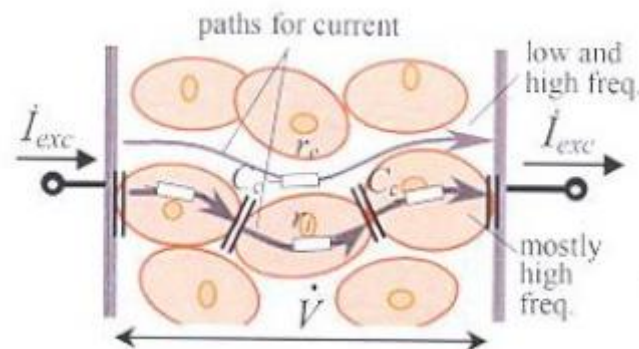


Figure 2.10 Comparison of the different paths followed by a current in an organic tissue depending on these frequencies [5]

This increase in conductivity is associated with a decrease in permittivity, from a high value at low frequency into three main relaxations: α , β and γ such as shown in figure 2.11. Each of these steps characterizes a type of relaxation that it occurs in a specific frequency range and it is characteristic for each tissue [4] [6].

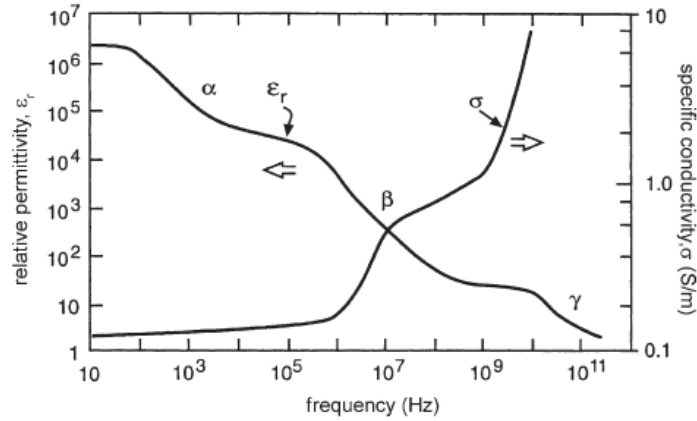


Figure 2.11 Frequency dependence of the dielectric parameters of biological tissues [7]

This thesis will cover the β relaxation area, comprising the frequency range of tens of kHz to hundreds of MHz and wherein the soft tissues are located. The β relaxation is the one most closely related to the properties of the cell membrane and the form of grouping the cells into various tissues.

The complex conductivity (σ) and the complex permittivity (ϵ_r), electrical properties of the tissues, are tensors, but if we consider that the tissue is isotropic, linear and independent in time, they can be considered scalar values depending on the frequency.

Tissue can be modelled using a two-terminal electrical circuit, which represents the impedance of the tissue studied. These electric models called 'lumped parameter models' allow a physical or physiological interpretation of bioimpedance.

These models are created from a cell immersed in an ionic medium, figure 2.12. In which the intracellular medium resistance and extracellular, the capacity of the cell membrane and its resistance are contemplated [8].

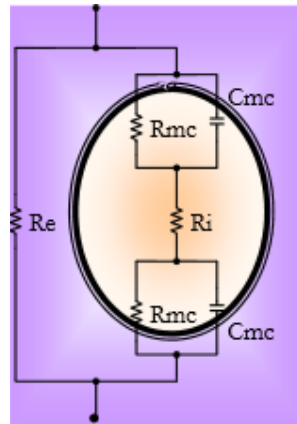


Figure 2.12 Model representing the main mechanisms that determine the impedance of a cell suspension.

There are other representations of electric models, such as the models that meet the complex permittivity Debye equation:

$$\varepsilon^*(\omega) = \varepsilon_\infty + \frac{\varepsilon_s - \varepsilon_\infty}{1 + j\omega\tau}$$

Equation 2.1 Debye equation

In which ε_∞ and ε_s are the permittivity at high and low frequency respectively and τ is the relaxation time.

The figure 2.12 shows the electrical representation, where R2 represents the resistance at low frequency, and high frequency resistance is the parallel equivalency of R1 with R2. This representation is useful for modelling tissue impedance with commercial components when testing the measuring equipment is required.

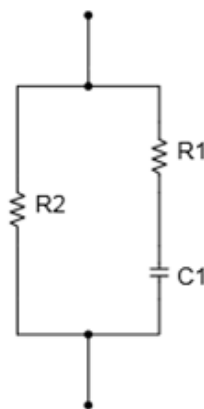


Figure 2.12 Equivalent electrical circuit of the Debye equation (with relaxation and $\alpha = 0$)

However, because biological tissues are heterogeneous media which involves several time constants, the most commonly function used to represent this situation is the one called Cole-Cole permittivity equation:

$$\varepsilon^*(\omega) = \varepsilon_\infty + \frac{\varepsilon_s - \varepsilon_\infty}{1 + j\omega(\tau_c)^{(1-\alpha)}} - j \frac{\sigma_s}{\omega\varepsilon_0}$$

Equation 2.2 *Cole-Cole permittivity equation*

Where α is a characteristic empirical parameter of the relaxation frequency distribution, f_c ($\tau_c = \frac{1}{2\pi f_c}$), showing the grade of dispersion of the time constants associated with relaxation phenomena . Thus, there is a similar expression for the impedance:

$$Z = R_\infty + \frac{R_0 - R_\infty}{1 + j\omega\left(\frac{1}{2\pi f_c}\right)^{(1-\alpha)}}$$

Equation 2.3 *Cole-Cole impedance equation*

And their representation in an electric model and the characteristic equations are shown in the figure 2.13.

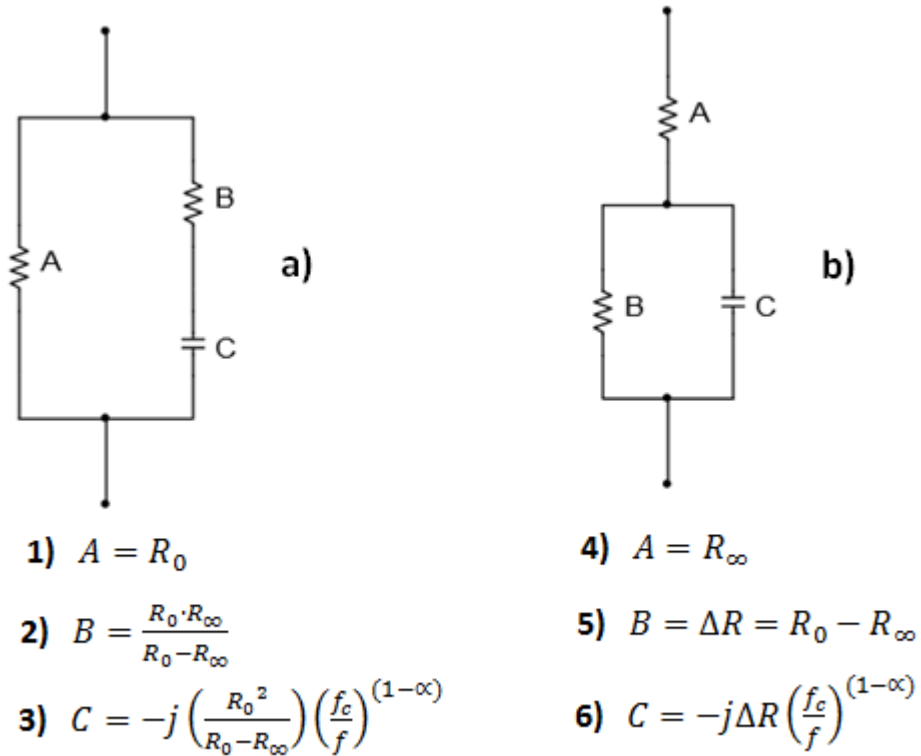


Figure 2.13 *Electrical circuit model of Cole-Cole equation*
 Equations 1), 2) and 3) correspond to the figure a)
 Equations 4), 5) and 6) correspond to the figure b)

Both the Debye model as the Cole- Cole, it can be found a more detailed description in [4] and [5].

The electrical circuits of the figure 2.13 b) are used during the setting stage of the measurement setup developed in this work.

2.7 Electrical Impedance Tomography

Electrical impedance tomography (EIT) is a technique used to produce static or dynamic images related to the conductivity distribution of the measured region. The advantages of EIT as compared to conventional imaging techniques such as computed tomography or magnetic resonance imaging are: It is considered safe by merit of the small alternating currents required; it can be used as a long-term, continuous imaging method; and the system can be constructed at low cost and in portable size [9] [10].

EIT has numerous practical applications, e.g. in quality control and fault detection for various materials [11], geological exploration [12] and medical imaging, [13] [14]. In present days, EIT has been extensively researched in medical applications [15]. The possible medical applications for EIT are monitoring for lung problems, such as accumulating fluid or a collapsed lung, non-invasive monitoring of heart function and blood flow, monitoring for internal bleeding, screening for breast cancer, studying emptying of the stomach, studying pelvic fluid accumulation as a possible cause of pelvic pain, quantifying severity of premenstrual syndrome by determine the amount of intracellular versus extracellular fluid, determining the boundary between dead and living tissue [16].

In medical applications, because of the differences in bioelectrical properties between tissues, the impedance distribution can indicates the structural and functional properties of the object. In EIT, the current flow is determined by the impedance distribution within the object. As well, the problem is ill-posed which meaning that large changes in impedance at the interior of the object can result in only small voltage changes at the surface [16].

In EIT the fundamental problem in the image reconstruction is that, in a general case, the electric current cannot be forced to flow linearly (or even along a known path) in an inhomogeneous volume conductor; the current flow is determined by the impedance distribution within the object or sample under test [17].

The reconstruction is possible due to the several four-terminal measurements carried out by the electrodes located nearby the sample under test, following the data collection strategy required. Therefore, these images are reconstructed according to the known stimulation current and measured voltage data, which means that the noise and the small errors in the measured data can cause large errors in the resulting images [18]. Hence, the accuracy of the measurement equipment has a great importance.

2.7.1 EIT System Architecture

While there are many different EIT system designs, most systems apply currents and measure voltages and can be classified according to the number of current sources, either as a single source system or a multiple source system. The system presented in this thesis will be single source. The general structure of an EIT system using a single source is shown in figure 2.14.

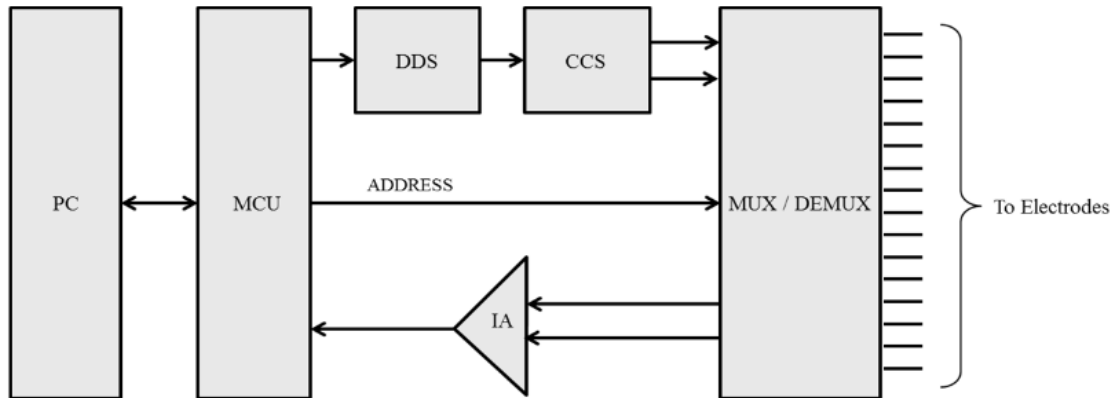


Figure 2.14 Diagram of a single source EIT system [19]

The waveform is produced by the DDS (Direct Digital Synthesizer) block. The waveform is fed to a dual current source or dual voltage-to-current converter, which produces a pair of currents having equal magnitude but opposite polarities. A multiplexing system allows these sources to be applied to one pair of electrodes at a time. The currents are supplied to the electrodes through shielded cables in which a driven shield is used to protect the signals from noise, as well as to minimize the cable capacitance and capacitance variation when the cables are flexed. Electrode voltages are measured using either single-ended or differential voltmeters [19]. Differential voltage measurement will be the one chosen for our application.

In addition, it is possible to use several current sources and voltmeters reducing the measurement time and eliminating the multiplexing system at the expense of more hardware, but it will depend on the needs of each particular EIT system.

2.7.2 Frequency range

The speed at which measurements will be performed is limited by the lowest frequency of measurement employed, since it should be assumed that a number of periods of excitation would be required for demodulation. In consequence, data acquisition for a complete image requires a minimum of 100 periods of the minimum frequency signal.

Two factors affect the choice of minimum frequency. First, the biological sample's impedance may be affected by temporary factors, the life of the stem cells under study is long enough to not to determine the frequency of measurement. Secondly, a frequency must be chosen that is above the frequency range in which the capacitive respond of the biological sample is present. This frequency would generally vary between 100KHz and 1MHz, depending on the sample.

In practice, the upper frequency limit for EIT is determined by available technology, since problems such as stray capacitances of only a few pF introduce significant errors [20].

2.7.3 Error sources

Because of the stray capacitances can determine significantly the EIT performance, it is essential identify those error sources.

EIT is performed using an array of contacting electrodes connected to a number of bioimpedance measurement channels. Errors between the channels are important as they can critically affect image quality. The accuracy of the EIT system will have to be higher for the static dynamic imaging (our case) rather than dynamic imaging. The equivalent circuit (figure 2.15) neatly introduces the EIT measurement problem for the case of application of constant current [21]

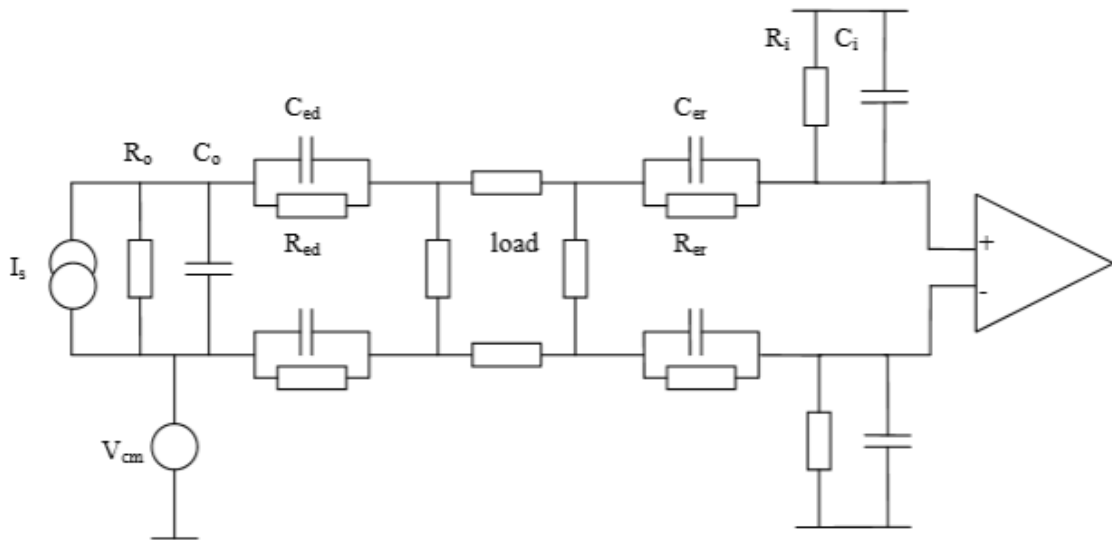


Figure 2.15 Equivalent circuit of the EIT measurement problem [21]

The major sources of error are caused by the common mode voltage (V_{cm}), the stray capacitance of the cables and switches (C_o, C_i) and the contact impedance between the

system and the impedance of interest (R_{ed} , C_{ed} , R_{er} , C_{er}). Hence, this model should be taken in consideration for the selection of those critical components

2.8 Data Collection Strategy

The EIT system resolution will be determined by the distribution of the electrodes around the sample and the measurement strategy. Several data collection strategies, i.e. collections of current injection and voltage measurement pairs, have been published. Below, there is a brief overview about the existing methods for a 16-electrode configuration.

2.8.1 Neighbouring Method

The neighbouring method, it is also called as the adjacent drive method. In this method, the current is applied through adjacent electrodes and the voltage is measured sequentially from all other adjacent electrode pairs without the pairs containing one or both the current electrodes [16]. The neighbouring method is the least sensitive in the centre as compared to the others, but its proportional selectivity is the best [10]

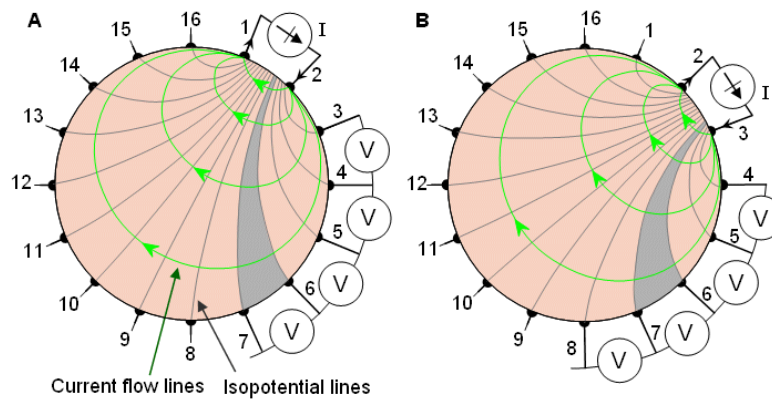


Figure 2.16 Neighbouring method of impedance data collection [17]

The neighbouring method shows a high sensitivity distribution when it is performed with 4 electrodes side by side, figure 2.17.

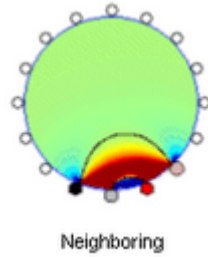


Figure 2.17 Sensitivity distribution of the Neighbouring method [10]

2.8.2 Opposite Method

The opposite or polar drive pattern applies current through electrodes that are 180° apart while voltage differences are measured on the remaining electrodes. Hence, this method is known as Opposite Method. Voltage differences are measured on the voltage electrodes with respect to the electrode (called as the voltage reference electrode) adjacent to the current-injecting electrode [16].

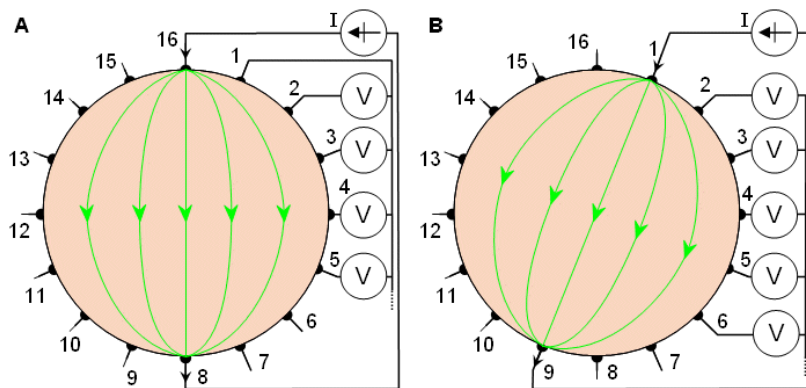


Figure 2.18 Opposite method of impedance data collection [17]

2.8.3. Cross Method

The cross or diagonal drive pattern is rarely used. In the cross method, adjacent electrodes are selected as current and voltage references. A more uniform current distribution is obtained when the current is injected between a pair of more distant electrodes [10].

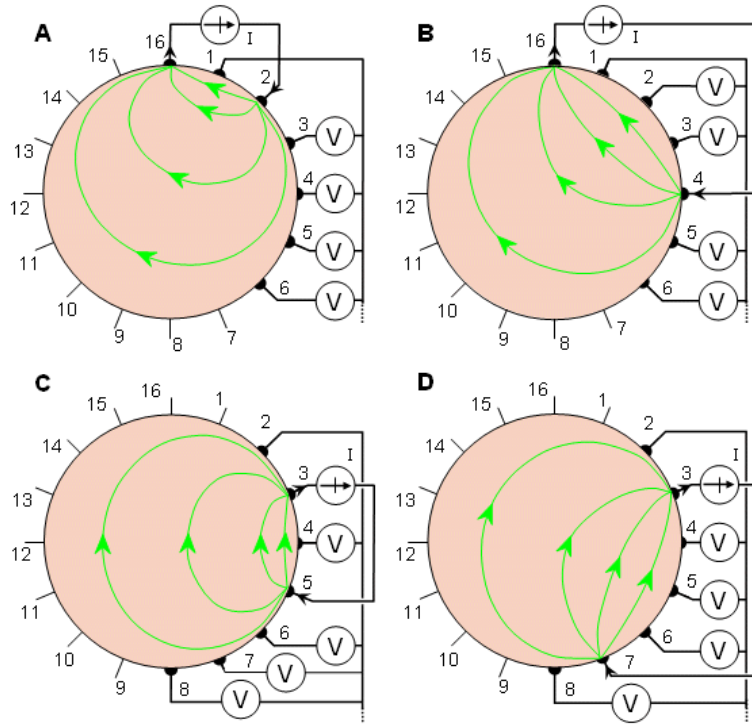


Figure 2.19 Cross method of impedance data collection [17]

2.8.4 Adaptive Method

In the adaptive method, current is injected through all electrodes. Because current flows through all electrodes simultaneously, as many independent current generators are needed as are electrodes used. Only in a homogeneous volume conductor a homogeneous current distribution may be obtained. The picture below shows the measurement strategy followed in this method.

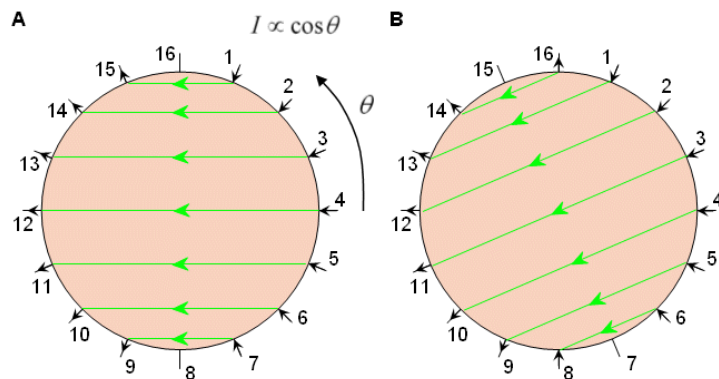


Figure 2.20 Adaptive method of impedance data collection [17]

The adaptive method produced most homogeneous sensitivity throughout the model. However, between the opposite, cross and the adaptive methods the values did not vary largely [10].

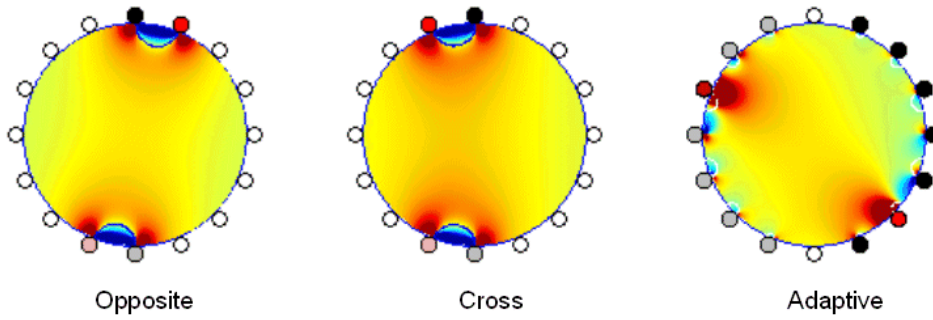


Figure 2.21 *Most sensitivity configuration detect centre region of the model* [10]

3. EIT INSTRUMENTATION

This chapter is divided into two parts; an introduction of the measurement setup used during this thesis, and the alternative setups with a completely different electronic instrumentation.

3.1 Measurement Setup

The measurement setup used for the test performed in this thesis is shown in the figure 3.1, based on an HF2IS Impedance Spectroscopy (Zurich Instruments), a digital Input/Output breakout board (available upon request by Zurich Instruments), a MUX system (CD74HC4067, Texas Instruments), the topology of electrodes shown in the section 3.1.4, and a LabView Program or the ZiControl application provided by the manufacturer.

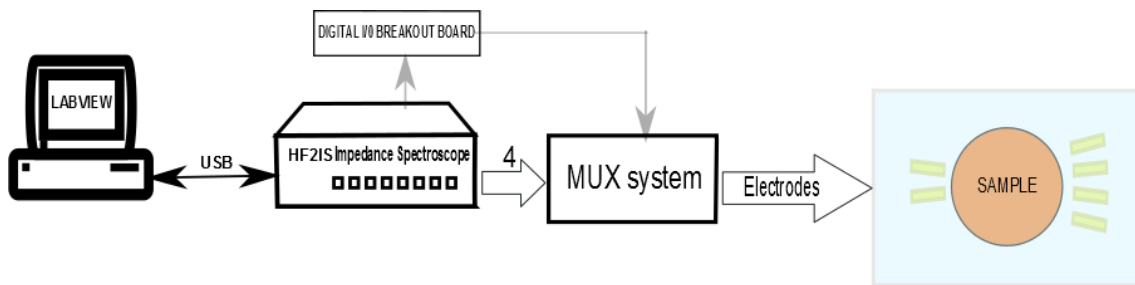


Figure 3.1 Measurement setup diagram

3.1.1 Impedance Spectroscopy

The HF2IS impedance spectroscopy is used for signal generation and voltage measurement, and it is represented in figure 3.1. This system has two separate input and output channels and can operate on a frequency range from 0.7 μHz to 50 MHz [22]. For higher precision, a current amplifier HF2TA (Zurich Instruments AG, Switzerland) can be used in conjunction with the HF2IS instrument. These components are controlled by ziControl (Zurich Instruments AG, Switzerland).

BNC cables, with 1 meter length each, are used in all connections, except the Ethernet cable between HF2IS and HF2TA and the USB 2.0 cable connecting HF2IS to PC. The length of the cables that leave from the MUX system to the electrodes has to be taken in consideration because they will increment the total length, and therefore the lead impedance.

The coaxial cabling impedance (R_L and L_L , figure 3.4) will affect to the measured value at frequencies higher than 1MHz. This can be minimized using shorter cables during the measurement process.

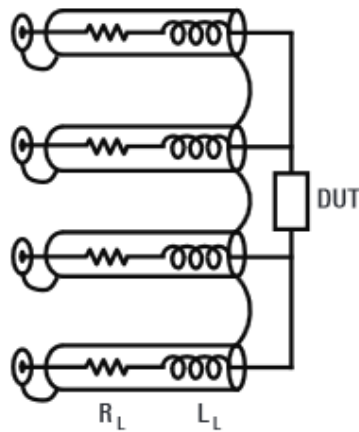


Figure 3.4 Coaxial cabling impedance

3.1.2 Multiplexing system

The EIT requires measure automatically from different points. Therefore, a multiplexing system has to be connected after the current injector and voltage measurement modules. The following commercial systems have been taken in consideration, but at the end, an own system based on 16x1 channels multiplexer has been used. These commercial systems could be suitable equipment for next stages of the project.

- **LinkBone 1-to-15 BNC Dual switch**, is an analog multiplexer/switch designed for switching digital and analog signals between a common port and 15 channels. All lines route electrical signals bidirectionally between ports [23].

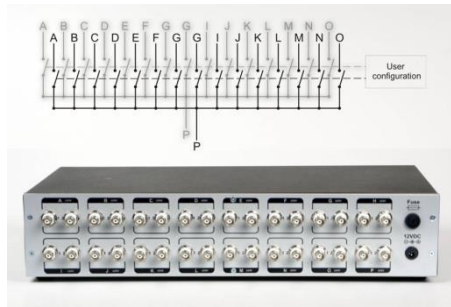


Figure 3.5 LinkBone 1-to-15 BNC Dual switch [23]

Advantages:

- BNC connectors
- 50 Ω channel impedance
- Two line 1-to-15 internal switching network
- Sufficient bandwidth
- Low price and signal degradation

Disadvantages:

- Two switchers needed
 - Less flexible configuration
 - Lack of LabView library
- **G2 series switching system**, which consists a G2T400 2RU mainframe with touchscreen control, and 2x G2R16-21X8-25 modules, totaling four 1x8 mux switches [24].



Figure 3.6 G2 series switching system and mainframe [24]

Advantages:

- BNC connectors
- 50 Ω channel impedance
- New modules for the future needs

Electronic Instrumentation for a 3D EIT Application

- Sufficient bandwidth
- Possibility of MxN configurations
- LabView programming

Disadvantages:

- Higher price
 - Expense on the mainframe
 - Several modules needed depending on the configuration
- **PXI matrix module 2541** with a 8x12 configuration from the manufacturer National Instruments [25]. This module will be easily expandable and more flexible for the different configurations during the measurements. As the G2 Series, a chassis will be needed, and in this case the PXI-1042 is a suitable option.



Figure 3.7 PXI matrix module 2541 and mainframe [25]

Advantages:

- BNC connectors
- 50 Ω channel impedance
- Expandable modules
- Sufficient bandwidth
- Matrix modules more flexible than multiplexers
- LabView programming

Disadvantages:

- Higher price
- Expense on the chassis

- **CD74HC4067 16x1 multiplexer** (Texas Instruments) is the option chosen for the multiplexing system due to the simplicity of working with them, low price and the breakout board from the manufacturer SparkFun Electronics.

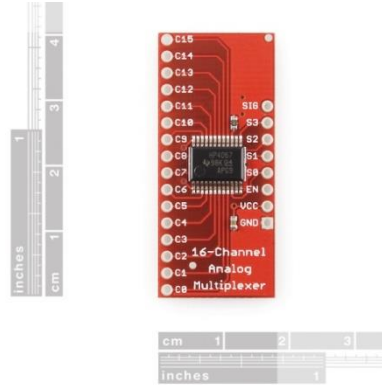


Figure 3.8 Multiplexer CD74HC4067

The internal resistance or ‘On’ resistance is 70Ω and the input/output stray capacitance of the channels is 50pF .

The figure 3.9 shows the distribution of the four 16x1 multiplexers. The common terminal is connected to each terminal of the HF2IS, following the scheme shown in the figure 3.3, and the 16 channels of each multiplexer are connected to the electrodes. The switching will be controlled by the DIO port of the spectroscopy through a breakout board.

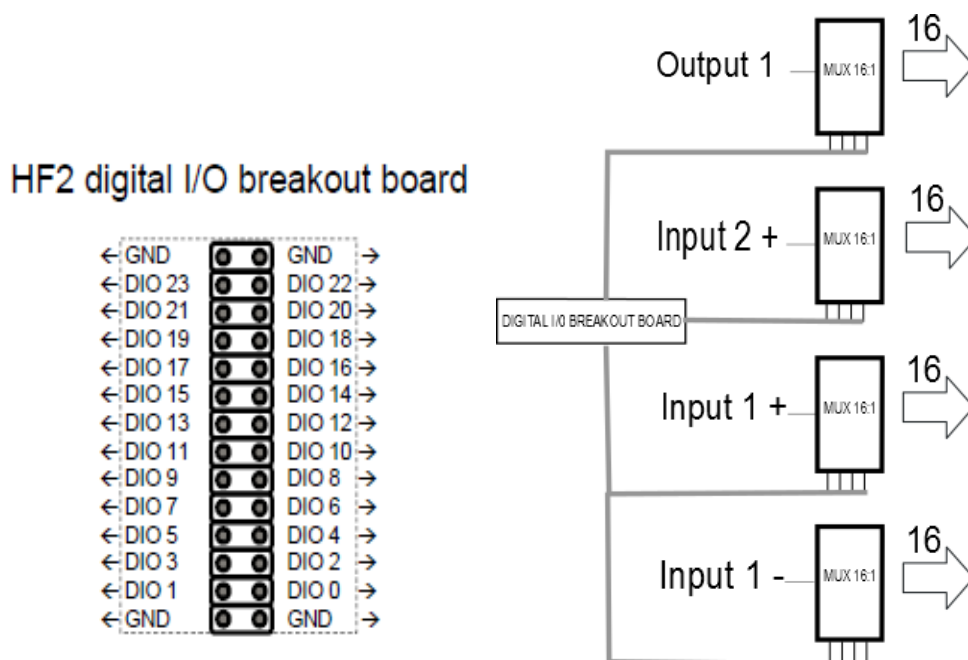


Figure 3.9 Digital I/O breakout board [22] and multiplexing system connection

3.1.3 Software: ziControl & LabView

The software used in the measurements is ziControl (Zurich Instruments AG, Switzerland). It is graphical user interface for accessing the HF2IS. It provides full control, several data visualization tools, data and setting storage, status and log functionality. ziControl supports local instruments (connected to the local computer over USB) or remote instruments (connected over TCP/IP) [22]. The panel configuration used is the explained in [26] for the four-terminal case.

Most importantly, the ziControl supports access to your HF2LI by multiple programs running in parallel (LabVIEW VIs, C++ based programs, Matlab, and others). Therefore, a LabView program can run simultaneously for an automatic process of measurement.

The tests shown in the chapter 4, have been performed using just ziControl (15.01v), but a LabView program is been tested based on the example LabView programs provided by Zurich Instruments (see Appendix 3).

Modifications of the LabView program can be used for automating the process, but ziControl will have to run in parallel anyway. On the other hand, the conventional imaging reconstruction algorithms are based on the values the current injected through two electrodes and the voltage measured through another two, although the impedance measurement values are useful during the first stages of the EIT system development, in the final prototype the values of interest will be both the current and the voltage. Besides the DIO switching, and therefore the multiplexing, will be limited to about 100 Hz only due to the software and USB latency.

3.1.4 Electrode location

About the electrodes location in the system, the data collection methods presented in the chapter 2.8 and the research [10] and [27] have been analysed. The mathematical models presented, and its conclusions, will determine the distribution of the measurement electrodes and the data collection strategy of the EIT system. Besides, the electrodes must not surround the sample because of there will be an optical imaging system working at the same time.

Although the rotation of the sample has not been developed yet, the electrode location has been designed considering this future technique. Therefore, the setup designed is composed of 6 electrodes per layer, figure 3.10.

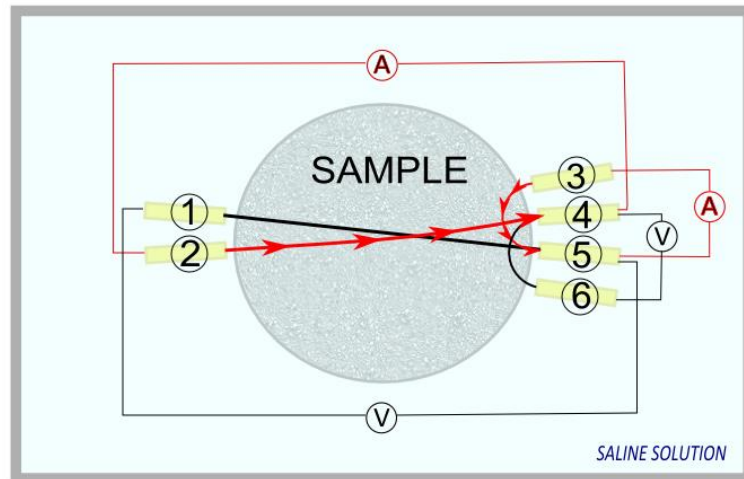


Figure 3.10 *Electrodes location in 2D*

Due to the sample will rotate during the tomography process, with just 6 electrodes, the data collection can be as good as in 16-32-64 electrodes configuration, where the electrodes are surrounding the sample forming a circumference. The rotation is indispensable due to the EIT system will be coupled to an optical imaging system, and as a consequence, the electrodes cannot surround the sample. Anyway, the electrode location will be open to future modifications during the development of the reconstruction algorithms for 3D imaging.

The methods used are opposite and neighbouring method, but unlike in the cases seen in the chapter 2.8, the voltage measurement and the current feeding are crossing during the performance, as in the cross method.

The electrode setup for the 2D system has been designed by the PhD researcher Mari Lehti-Polojärvi. It is built with PLA material and gold electrodes. It is a sealed container where the electrodes are fixed 1cm around the sample in the desired position. The container must be sealed because the sample is submerged in a saline solution.

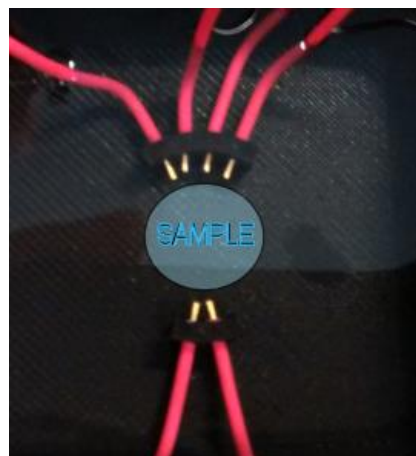


Figure 3.11 *Electrode setup 2D*

3.2 Alternative measurement setup

The main issue of the measurement shown before is that the HF2IS is utilized for just a simple task, between all the possibilities that offers, which it is a waste of resources for a final prototype. Besides, the DIO switching will be limited to about 100 Hz only due to the software and USB latency and therefore, the multiplexing frequency. As a result of these problems, it is important to plan which components would be required to design a customized single-source EIT system without the help of the HF2IS. The figure 3.12 shows a scheme of the different blocks which form the hardware of the EIT system.

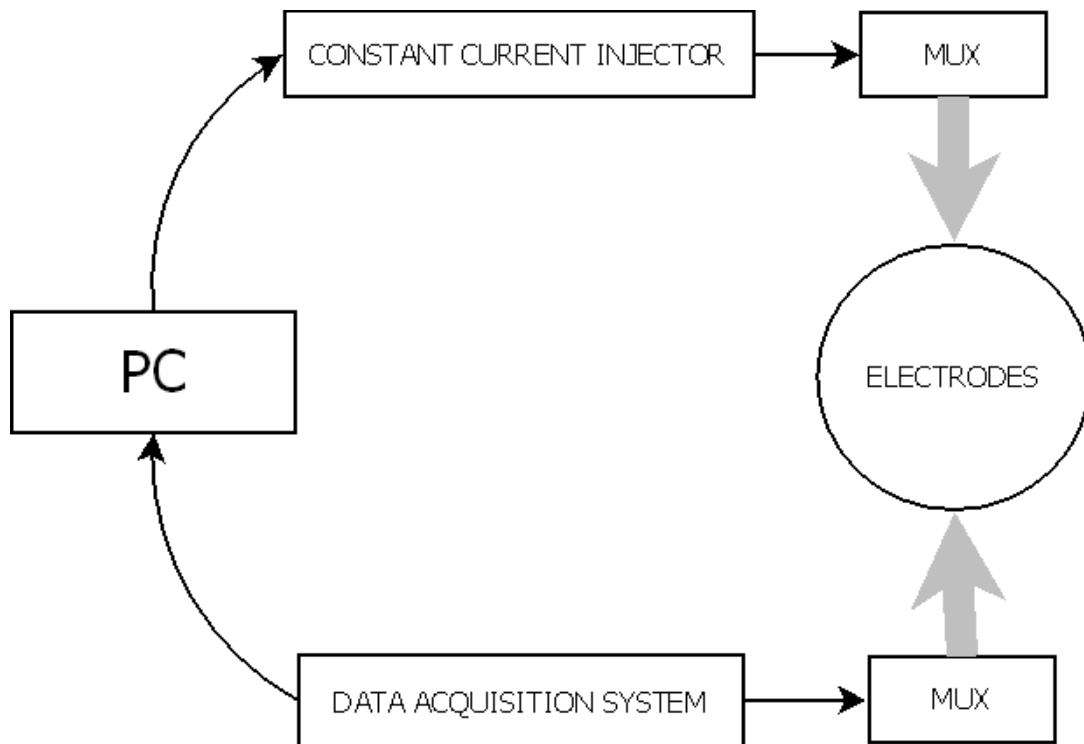


Figure 3.12 Block diagram of an EIT system

Basically, the setup is based on a constant current injector, MUX system like the one used during the tests and a Data Acquisition System. Therefore, a brief study of these components is detailed below.

3.2.1 Constant current injector

The constant current injector can be divided in two parts, the waveform synthesizer to produce the sinusoidal waveform at the frequency desired and the current source, in charge to 'convert' that sinusoidal wave from voltage to current.

- **Direct Digital Synthesizer (DDS)**

A Direct Digital Synthesizer (DDS) is a digitally-controlled method of generating multiple frequencies from a reference frequency source [28].

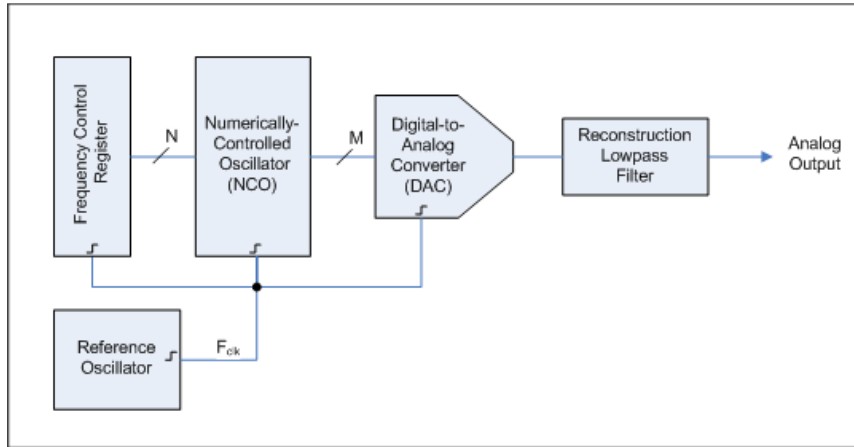


Figure 3.13 Block diagram of a DDS

A DDS system is constructed around a sinusoid ROM lookup table. A phase increment, $\Delta\Phi$, is fed into a phase accumulator that, in turn, provides addressing to the lookup table. The size of the phase increment along with the clock frequency sets the output frequency [2].

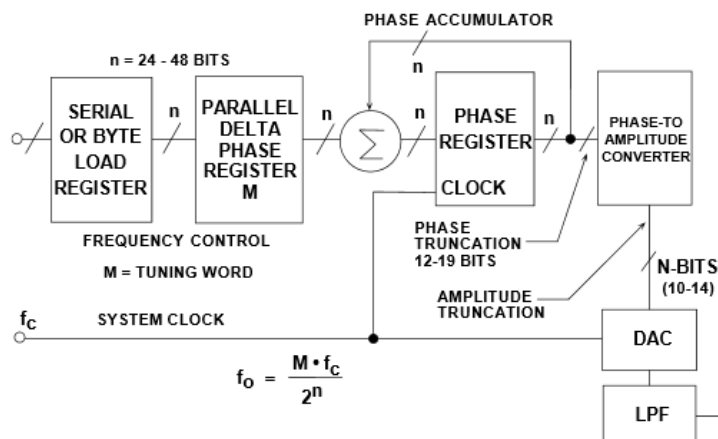


Figure 3.14 Internal operation of the DDS [28]

The phase accumulator content is updated once each clock cycle. Afterward, the digital number, M , stored in the delta phase register is added to the number in the phase accumulator register every clock cycle. The truncated output of the phase accumulator serves as the address to a sine (or cosine) lookup table, which will contain 1/4 cycle of the sinusoid. Hence, the lookup table maps the phase information from the phase accumulator into a digital amplitude word, which in turn drives the DAC. As a result, the frequency of the output sinewave is equal to:

$$f_o = \frac{M \cdot f_c}{2^n}$$

Equation 3.2 *DDS ‘tuning equation’*

At the time to select a commercial DDS, the AD9850 from Analog Devices is an integrated device used for test and medical equipment [19] and based on advanced DDS technology. With a reference frequency of 125 MHz (f_c) it is able to generate output frequencies of up to one-half the reference clock frequency, 62.5 MHz (f_o). The tuning word (M) is compounded by 32 bits (n). These characteristics should fulfil the requirements, albeit if they were insufficient, there are more advanced models as the AD9838.

- **Current Source**

The current source in an EIT system must be able to deliver current through the current electrodes with a desired precision at a specified frequency range.

More than a typical current source, what is commonly used in EIT is a voltage-to-current converter, which produces an output current proportional to the input voltage supply by the DDS shown previously. According to [2], the following criterions should be the ones taken in consideration for the design of the current source and in the case of a general EIT setup.

- Current amplitude should be as large as possible without compromising safety.
- The specified output impedance (Z_o) is almost always greater than 1 M Ω .
- The relationship between control voltage and output current (transconductance) should be linear.
- The source should introduce minimal common-mode voltage into the measuring circuit.
- For multiple-frequency imaging, the design should meet the specification of the above factors over the design frequency-range.

In this case of static imaging, the output impedance has a great importance due to the high accuracy required by the static imaging. On the other hand, minimizing the common-mode voltage will be more important for the dynamic imaging [2].

There are many current sources that are used in EIT systems, but for single source EIT system, the one presented in this thesis, the most common is the floating current source. Therefore, many commercial current sources can be considered as suitable candidates, as the LT3092 (Linear Technology, USA).

An often used current source is a Howland current pump, which relies on matching between resistors to achieve high output impedance. An ideal current source would have infinite output impedance; thus, all the current delivered must flow through the load [21]. There are many publications about the Howland current source in EIT systems [29] and other alternatives [30].

The example of a modified Howland VCCS from [29] is shown below:

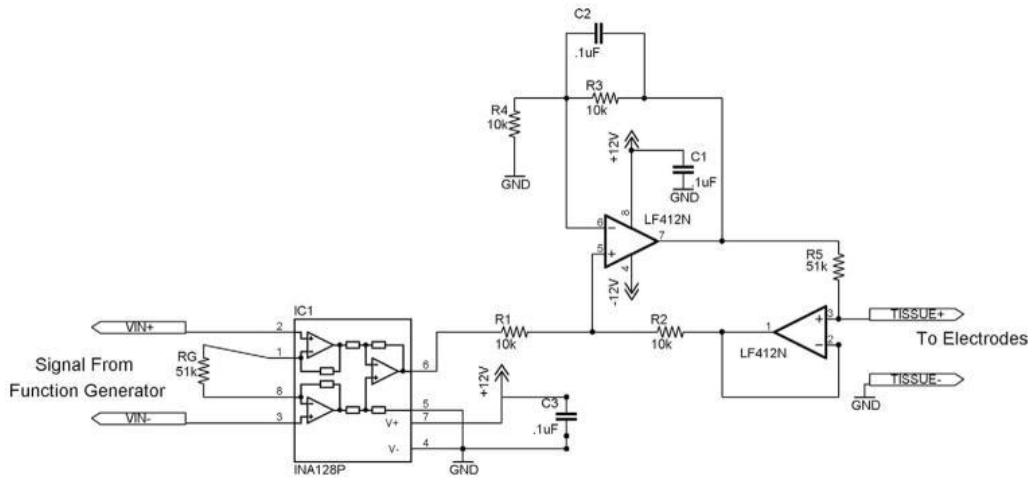


Figure 3.13 Modified Howland VCCS

The circuit is composed of 2 stages, the first being an instrumentation amplifier (INA128P) that acts as a preamplifier and eliminates any common mode noise present in the input signals. The second stage is the Howland current source circuit. The expected transfer function for the circuit is $I_{\text{tissue}} = 2 \cdot (V_{\text{in}}/R_5)$.

3.2.2 Multiplexers

The tests developed for this thesis have been performed using the HF2IS, therefore only a single current source. In this case, the use of multiplexer is essential as it has been shown before.

These devices have many non-ideal properties that make them undesirable in EIT systems, including a nonzero ‘on’ resistance that is somewhat dependent on the applied voltage, limited ‘off’ isolation, with lower values at high frequencies, and charge injection during switching. The most significant problem, however, is the relatively large capacitance of multiplexer devices. Typically the input capacitance is in the range 30–50 pF and the output capacitance on each line is in the range 5–10 pF.

Multiplexers made using smaller devices will have lower capacitance values at the cost of higher ‘on’ resistance [31].

Considering those requirements, the table 3.1 shows a comparison between two 1x16 channels multiplexer, the one selected for the MUX system used in this thesis (CD74HC4067, Texas Instruments), and another alternative with lower R_{on} (ADG706, Analog Devices) .

	R_{on}	C_i/C_o * ¹
CD74HC4067	70 Ω	50 pF
ADG706	2.5 Ω	200 pF

*¹ Input and output capacitance value.

Table 3.1 General specifications of the 16-channels multiplexers

The second model has a lower ‘on’ resistance due to his smaller size, but otherwise the ‘on’ capacitance is four times bigger than in the CD74HC4067 model. Therefore, the R_{on} of the multiplexers cannot be completely minimized in order to have a low ‘on’ capacitance.

The stray capacitance will be undesirable and harder to compensate than the R_{on} . Hence, it is recommendable to select the multiplexer with the lower C_i/C_o .

3.2.3 Cable shielding

The electrodes are located at some distance from the electronics and therefore, they have to be connected using cables of a considerable length. In order to minimize the coupling between the signals from different electrodes and reduce the noise susceptibility, coaxial cables are required. Due to their much higher output impedance, current source outputs are much more susceptible to noise pick-up than voltage source outputs and need protection [31].

These coaxial cables typically present stray capacitance the order of 40–100 pF/m, due to the shield. In addition, the capacitance tends to vary, particularly with the flexion of the cable. The shield is commonly driven with a voltage that is nearly equal to that on the conductor, figure 3.14. The voltage across the capacitance is zero, it does not carry current and is essentially removed from the circuit [31].

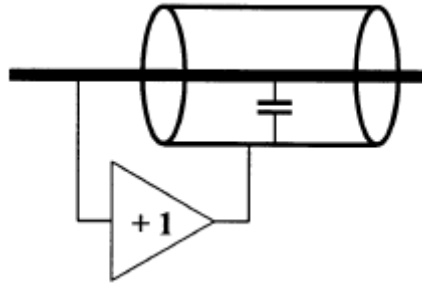


Figure 3.14 Coaxial cable shield connection

3.2.4 Data acquisition System

After the voltage electrodes it is located the Data Acquisition System, in charge of processing the differential voltage values. The figure 3.15 shows a scheme of the main parts which compound the system.

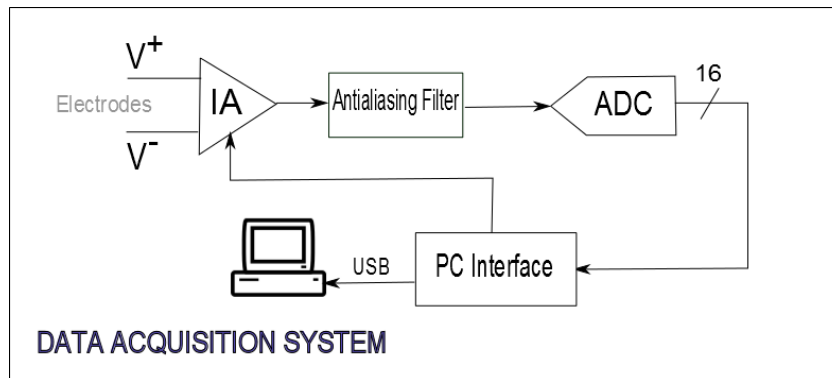


Figure 3.15 Data Acquisition System block diagram

The voltage measurement can be performed as a differential or single-ended voltage measurement. Considering the distribution of the electrodes and the voltage measurement performed shown in the figure 3.10, the IA should carry out a differential measurement. The analog signal is digitalized in an ADC. An antialiasing filter is located between the IA and the ADC to reduce undersampling issues.

An example of an IA which would fit our needs it is shown in [32], where it is designed an IA for EIT with a dynamic range of 85dB over a 10 MHz bandwidth. Other commercial IAs suitable for this EIT system could be the AD8421 Instrumentation Amplifier (Analog Devices Corporation, USA) and the INA111 Instrumentation Amplifier (Texas Instruments Inc., USA).

The AD7654 Analog to Digital Converter (Analog Devices Corporation, USA) fulfils the function of ADC in the Data Acquisition System. As antialiasing filter, the MAX7400 (Maxim Integrated, USA) would be a good choice.

Electronic Instrumentation for a 3D EIT Application

Instead of the ADC, it can be used a microcontroller as in [19], where it is selected the model PIC18F4620 (Microchip Technology Inc, USA).

An alternative to design the whole DAS is a commercial one, like the NI USB-6361 (National Instruments) which simplifies the system, allows an easier programming in LabView, provides a technical support and has a warranty period.

4 RESULTS

The results of impedance spectroscopy measurements are presented in the following subchapters. These preliminary tests are useful to the extent that it can be extracted useful information about the measurement setup, the multiplexing system in the whole range of frequency and the range of frequency where a biological sample, a carrot, shows his capacitive response (β , chapter 2.8). R-C circuits will simulate the bioimpedance of biological tissues.

The electrode system built in PLA material and designed by the PhD researcher Mari Lehti-Polojärvi is tested. Besides, the concentration of the saline where the hydrogel is going to be submerged has been established. The two methods of data collection for the EIT system have been tested too.

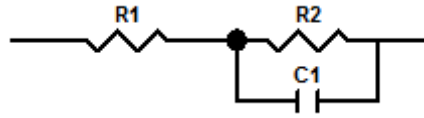
The results are focused on the 2D EIT case, but the information extracted from these tests is going to be of main importance for the development of the 3D EIT system.

This chapter can be divided in three parts, consider the three sort of sample under test:

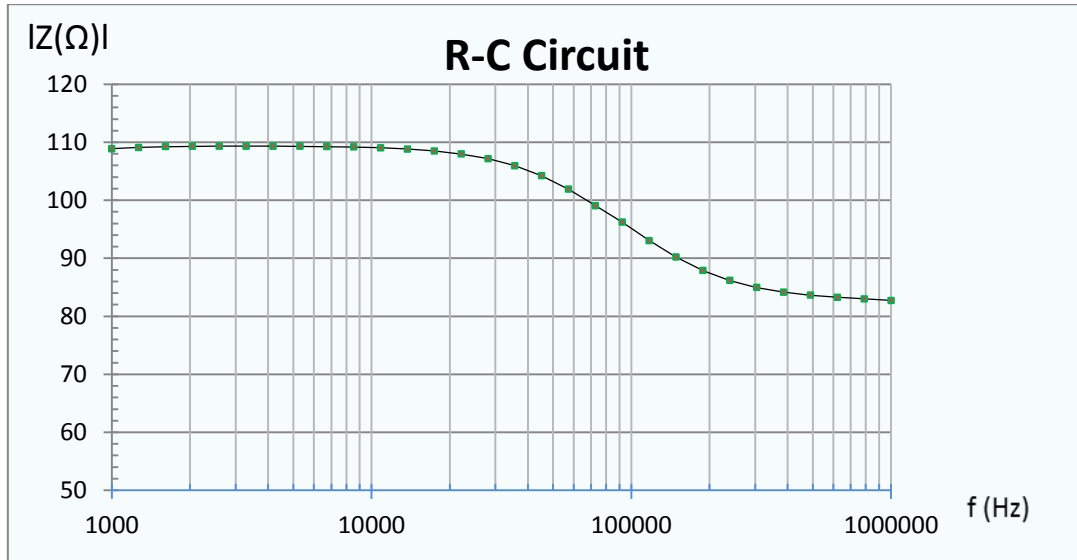
- R-C circuits
- Hydrogel
- Carrot

4.1 R-C circuits and evaluation of the measurement setup

First of all, it is need to test the measurement setup before measuring any biological sample. For that purpose, R-C circuits can simulate the capacitive behaviour of the biological samples. The figure 4.1 b) shows an impedance sweep using the HF2IS impedance spectroscope on an R-C circuit, figure 4.1 a).



a)



b)

Figure 4.1 a) R-C circuit ($R1=27\Omega$, $R2=82\Omega$, $C2=68nF$)

b) Impedance Spectroscopy of the R-C circuit

Next, the same R-C circuit has been measured, but this time using the MUX system shown in the chapter 3.1.2 . The figure 4.2 shows a comparison at a frequency range of 1 kHz - 1 MHz between the normal four-terminal impedance measurement without MUX system and with the multiplexers in between the electrodes terminals and the spectroscopie.

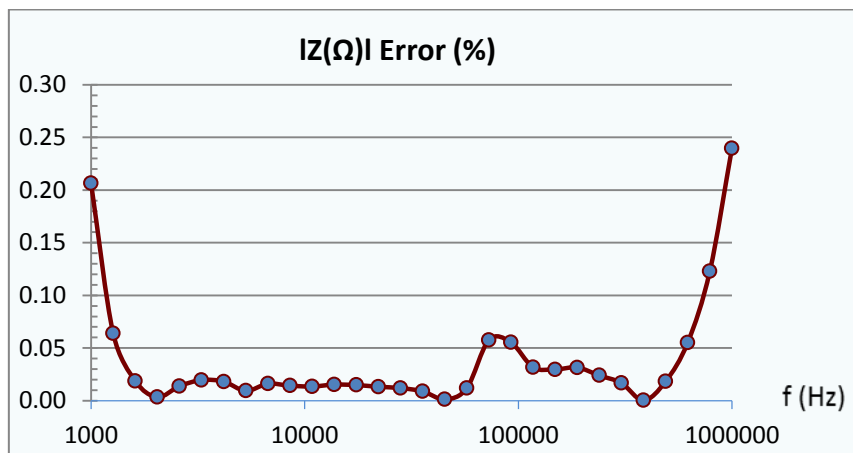


Figure 4.2 Error of the multiplexing system

It can be determined that the multiplexing system based on the 16x1 channel multiplexer CD74HC4067 do not introduce a big error in the impedance measurement (less than 0.25% at 1MHz) and most of this error might be due to the larger length of the cables used with the multiplexing, and therefore it will be constant for all of the measures with the multiplexing system. The Appendixes A and B shows a comparative table about the multiplexing system effect in the measured value. Therefore, the setup can be used for measuring the hydrogel and carrot samples. In the future, when a greater accuracy is required, the error can be reduced by calibration.

4.2 Hydrogel tests

The first tests using the electrode setup is with Hydrogel (composed of Gellan Gum Gel cross with calcium calcium) from the postdoctoral researcher Ana Soto de la Cruz in a PBS solution (1.5%) diluted in distilled water at 25 °C. This hydrogel will be used for TE applications as a scaffold for different types of cells, therefore its resistivity it will be of high interest. The figure 4.3 shows the 2D electrode setup with the hydrogel sample located in the centre.

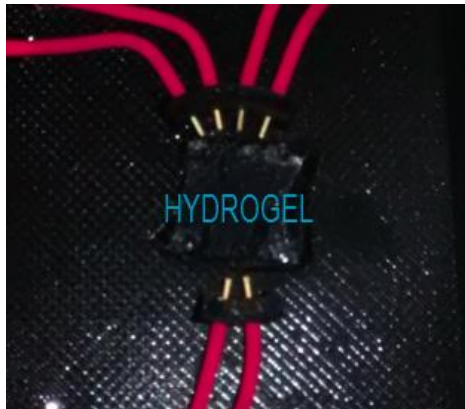


Figure 4.3 *Hydrogel test*

The procedure of measurement is done following both methods mentioned before, opposite and neighbouring method. The excitation signal is set to 25mV of amplitude. The measured value will greatly depend on the saline solution chosen, the distance between electrodes, their correct location and the hydrogel characteristics. The figure 4.4 shows the impedance sweep in frequency for both methods. As well, from 1 MHz the impedance value increases exponentially. This could be caused by the stray inductance of the cables, due to 1 meter coaxial cables have been used during the tests.

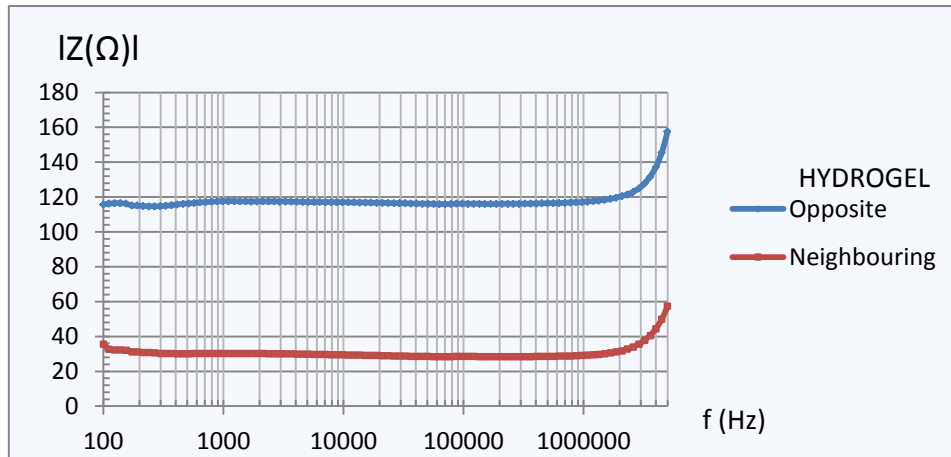


Figure 4.4 Impedance Spectroscopy Hydrogel

The graph shows the almost constant impedance value until frequencies of 1MHz. As well, the values in the neighbouring method are lower as it could be expected, due to the lower distance between the electrodes compared with the opposite method.

There are several studies with different types of hydrogels, e.g. in [33] the calcium cross-linked GG had an impedance value of about 1.2 kΩ at 36 °C, measured with two electrodes of distance 2.5 cm and averaged at 100 Hz – 100 kHz. The difference with our measurement can be caused by:

- Different composition of the gel
- Less distance between our electrodes, 1 cm for the opposite method
- There is a distance between the hydrogel and the electrodes
- The temperature in both tests is not the same
- Our system uses four-terminal configuration

From this test we can conclude that the impedance value of the hydrogel is about 120Ω at 25 °C, measured with four electrodes 1cm distance and along the frequency range of 1 kHz – 1 MHz.

4.3 Carrot tests

There are many EIT publications where biological samples as cucumbers, carrots or bananas are used for testing the EIT system [34] [35]. Next measurements are carried out over carrot samples with different shapes and sizes, in order to evaluate the change of the impedance value measured in each method. The solution in where the carrot samples are submerged has a lower conductivity than in the hydrogel test due to the higher resistivity of the carrot. The PBS solution is diluted in distilled water in a 1/200 proportion.

For the first test, a circular 9mm diameter piece of carrot has been measured, following the same procedure than in the previous test with hydrogel and an excitation signal with 25mV of amplitude.

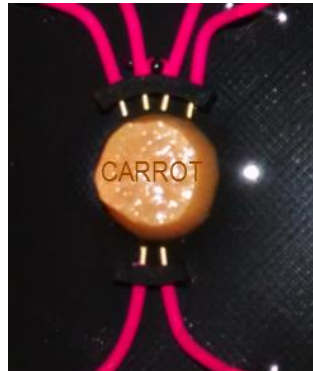


Figure 4.5 $\varnothing 9mm$ Carrot Test

The figure 4.6 shows a comparison between the performance of the opposite method measurement when the carrot is present, and when it is not (just the solution).

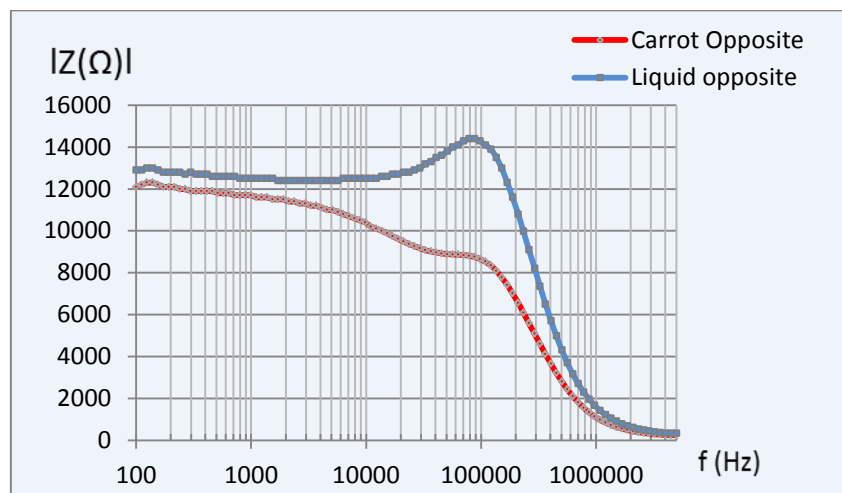


Figure 4.6 Impedance spectroscopy $\varnothing 9mm$ Carrot Test

The capacitive property of biological samples is palpable. At frequencies around 300-500 KHz the difference between both measurements is over $3k\Omega$, this is due to the decrease of the carrot impedance with the frequency, as in the tests performed with the R-C circuit. The values are similar to the one published in [35].

It is important mentioning that at low frequencies the values of both measurements should be quite similar, but the contamination of the solution with little particles of the carrot modifies its composition, thus the solution conductivity increase.

Then, the same procedure is followed for the neighbouring method as it is shown in the figure 4.7.

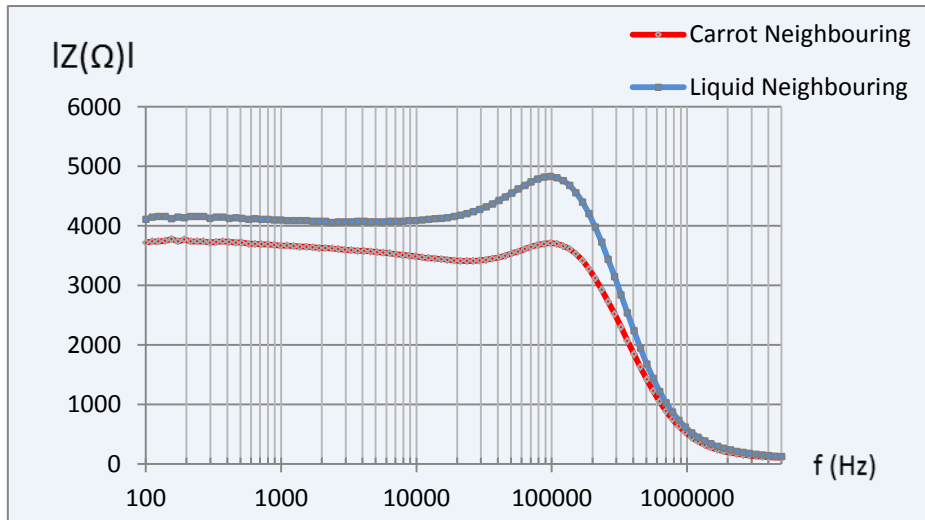


Figure 4.7 Impedance spectroscopy $\varnothing 9\text{mm}$ Carrot Test

As in the opposite case, the problem with the contamination of the solution appears at low frequencies, but anyway, the capacitive property of the carrot sample can be seen at frequency values around 300kHz.

Next measurement is carried out over a 4,5mm diameter carrot. First of all, it is important to stress that the values measured over the $\varnothing 9\text{mm}$ carrot, cannot be compared with the ones measured over the $\varnothing 4.5\text{mm}$ carrot because of the contamination of the solution during the process. This is not an impediment for these tests, but in next stages of the project will be determinant at the time of choosing the hydrogel composition, avoiding the mix with the solution.

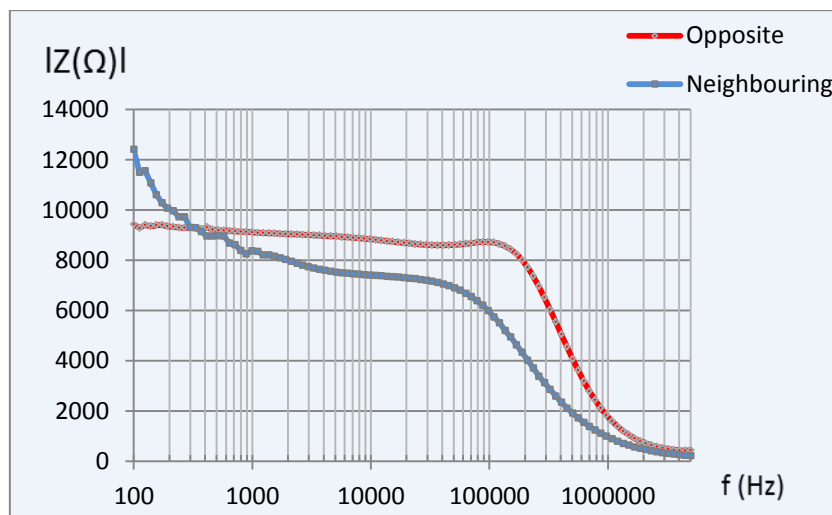


Figure 4.8 Impedance spectroscopy $\varnothing 4.5\text{mm}$ Carrot Test

The graph of the figure 4.8 shows the values of the opposite and neighbouring measure over the 4.5 mm carrot sample, being the decrease of impedance value around the same range of frequency as for the previous sample.

A final carrot measurement is performed with a 2mmx6mm rectangular sample. Two positions of the sample are analysed, a perpendicular position to the electrode setup (90°) and an alienated position respected to the electrodes (0°) (figure 4.9). The measuring procedure is the opposite method.

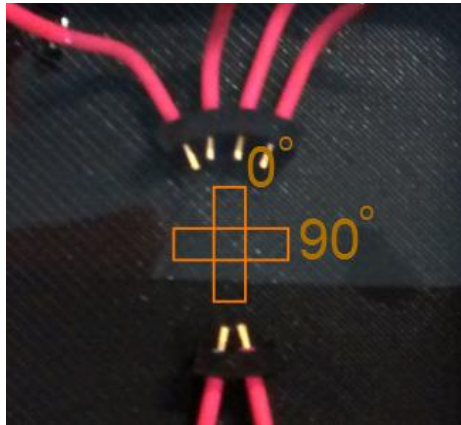


Figure 4.9 rectangular sample, 0° and 90° positions

The impedance sweep of the figure 4.10 shows that the values measured when the sample was located in the 0° position are lower than the ones of the 90° position. This is what it was expected, due to in the first case, the current flows through the sample more distance (the sample conductivity is higher). Therefore, for the 90° position measurement, the impedance values are higher.

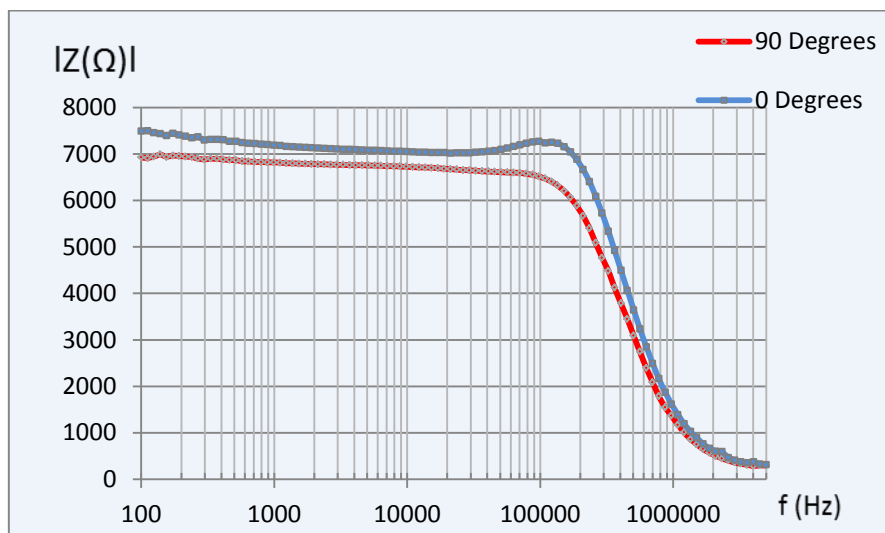


Figure 4.10 Impedance spectroscopy, rectangular sample

5. DISCUSSION

In this chapter the measurement setup and the main results are summarized and analysed. The future line of work will be presented in the next section.

5.1 Analysis of the measurement setup

The measurement setup used in this thesis is explained in the chapter 3.1, with the HF2IS Impedance Spectroscope as the main tool. This device performs the measurements with high accuracy in a range of frequency up to 50MHz, but in the tests, at frequency larger than 1MHz, the cabling impedance starts to distort the impedance measured.

The multiplexing system used to change from opposite to neighbouring method (chapter 3.1.2), have a right performance, as it is shown in the appendix A,B. In these tables, some irregular measurements are observed at certain frequencies. However, this may be caused by incorrect electrode connection, improper soldering or larger length of the cables in the multiplexing system.

In the section 2.7.3 there is a brief analysis of the error sources, but this topic has not been developed in depth because the measurement setup has shown repeatability enough for these first tests. The cables, the MUX system and the electrodes cause inaccuracies but those errors are constant in every measurement. Besides, it can be easily calibrated if necessary. In principle, this is not completely necessary for this development phase of the EIT system, because it is not required to have an exact impedance value but a high repeatability in the measurements.

The rotation during the tomography process is indispensable because the EIT system will be coupled to an optical imaging system, and as a result, the electrodes must not surround the sample completely. Thereby, the electrode location (chapter 3.1.4) is selected according to the theoretical studies presented in the chapter 2.8, so it will be open to future modifications during the development of the 3D imaging reconstruction algorithms.

5.2 Analysis of the results

In the chapter 4, different sorts of samples are measured with the purpose of increasing the knowledge about the measurement setup, the hydrogel resistivity, the solution in which the samples are submerged and the capacitive properties of the cells.

The solutions made of PBS diluted in distilled water depend on the sample under test, because its conductivity has to be slightly lower than the sample. The conductivity of the solution has to keep a stable value during the whole process of measurement as well. Therefore, it is important to avoid that any particles of the sample blend with it. This problem is shown during the measurements with the carrot (chapter 4.3). Taking this into consideration, the future hydrogels should have enough integrity to rotate and not to mix with the solution.

During the hydrogel tests, we obtained a resistivity value of 120Ω at 1KHz-1MHz for a 1cm distance between electrodes. This value differs with other impedance measurements on GG hydrogel, but this difference can be caused by several issues as explained in the chapter 4.2. Therefore, the test conditions will determine the value measured so it is crucial to keep them under control.

The observation from the carrot measurement proves the background presented in the chapter 2.8. The electrical circuit models will have the same capacitive response as the carrot cells at frequencies higher than 100 kHz. The excitation signal is a critical parameter because an excessively high excitation could kill the cells of the sample. During these measurements, the excitation signal has been injected amplitude values up to 25mV, a value which is not harmful for the cells. Hence, it has been possible to cross the cell membrane of the carrot cells with no damage.

The comparison of the different methods used in the data collection strategy has not given relevant information in quantitative terms. However in the first test with the 9mm \emptyset carrot, the capacitive effect seen with the neighbouring method is much smaller than with the opposite method. This can be easily explain due to the neighbouring method is focused on the periphery of the sample, being smaller the surface of carrot crossed during the measurement, and therefore, less cell membranes (capacitors) are measured.

5.3 Future work

As discussed in the chapter 3.2, the measurement setup used during the tests performed in this thesis (section 3.1) has some disadvantages, e.g. the DIO switching will be limited to 100 Hz only due to the software and the USB latency, as well as using the HF2IS Impedance Spectroscope for a final prototype which will be a waste of resources. As a consequence, the alternative measurement setup should be the line of work followed in the future design of the 3D EIT system.

However, the spectroscope performance has been satisfying. Hence, it is recommended for continuing doing conventional four-terminal impedance measurements, as in this thesis.

Moreover, the electrode location has been selected according to the theoretical models of the referenced publications, but a parallel work will have to be carried out during the reconstruction algorithms development.

The LabView program will have to be developed in depth when the rotation system is ready. This system has to be fairly accurate to rotate the sample until the position required with the least error possible.

6. CONCLUSION

In the first place, this thesis has been focused on the electronic instrumentation required for a 3D EIT application. The aim of the whole project, in which this work is included, is the imaging reconstruction of living cells covered with blank hydrogel. However, it has not been achieved because the project is in an early stage of development. Nonetheless hydrogel and biological samples have been measured.

The electrode location and the data collection strategy have been selected according to the authors referenced and their conclusions. Hence, it could be possible that they should not fit correctly for our project when the imaging reconstruction algorithms are ready.

From the results obtained in the chapter 4, the following conclusions are extracted: (1) the multiplexing system chosen (figure 3.9) fits our needs properly and does not distort the measurement in a significant way, (2) the test performed over the Hydrogel (composed of Gellan Gum Gel and calcium) give us information about its resistivity and the composition of the solution required, (3) in the measurements on the different samples of carrot, it is shown that the equivalent impedance model of biological samples can be represented by electric R-C circuits.

Moreover, the measurement setup used, figure 3.1, is mainly selected because of the availability and high performance of the HF2IS Impedance Spectroscope. On one hand, this device fits the requirements in terms of frequency range, and it can perform four-terminal impedance measurement. On the other hand, it is a versatile device capable to complete multiple tasks, and hence, used for another purposes in the department. Thus, it would be a waste of resources if it is used in a final prototype.

For that reason, it is possible to find a study of the components in the chapter 3.2, which would form an EIT system without the need of the HF2IS. It is a brief overview of the minimum requirements for the design of a single source EIT system as an aid to the development of the project as it was mentioned in the 'future work' chapter, although it requires a more detailed work for the construction of a prototype.

In conclusion, the purpose of this thesis is to carry out an analysis of the electronic instrumentation required for the EIT system described previously, concluding that the setup used for testing during this thesis is a good choice for continuing with the development of the electrode location and for working with the reconstruction imaging algorithms, but it would not be appropriate for a final prototype. At the same time, alternatives for the multiplexing system used during the tests have been proposed, based on commercial multiplexing systems which offer BNC connectors that

Electronic Instrumentation for a 3D EIT Application

facilitate the work with the system, and increase its flexibility during the EIT system development period. Hence, these systems should be taken into consideration for the upcoming equipment investment.

REFERENCES

- [1] Agilent Technologies, Inc., *Agilent Impedance Measurement Handbook, A guide to measurement technology and techniques*, 4th ed. USA, 2013, pp. 1-22.
- [2] K.G. Boone Holder D.S., *Current approaches to analogue instrumentation design in electrical impedance tomography.*, 1995, pp. 220-235.
- [3] David W. John W. Hill Rhonda J. Scott Ball, *Introduction to Chemistry. General, Organic, and Biological v. 1.0.*
- [4] B., Morucci, J.P., Chauveau, N. Rigaud, *Bioelectrical impedance. 1. Bioimpedance measurement.*, 2nd ed., 1996, ch. Impedance Spectrometry, pp. 257-351.
- [5] Martinsen O. Grimmes S., *Bioimpedance and Bioelectricity Basics*, 3rd ed., 2014.
- [6] K. , Schwan, H.P. Foster, *Dielectric properties of tissues.*, 1996, pp. 25-102.
- [7] Pavšelj N. , Hart F.X. Miklavčič D., *Electric Properties of Tissues.*, 2006.
- [8] A. Rabbat, *Electrical impedance tomography.*, 1990, ch. Tissue Resistivity, pp. 8-20.
- [9] Zhu Q., Lionheart WR., Lidzey F.J., McLeod C.N., Paulson K.S., Pidcock M.K., *An adaptive current tomography using voltage sources.*, pp. Sensitivity Distribution of Impedance 163-8.
- [10] Pasi Kauppinen, Jari Hyttinen, Jaakko Malmivuo, "Sensitivity Distribution Visualizations of Impedance Tomography Measurement Strategies," Ragnar Granit Institute, Tampere University of Technology, Tampere, Finland, 2006.
- [11] Jerome P.Lynch Tsung-Chin Hou, "Electrical Impedance Tomographic Methods for Sensing Strain Fields and Crack Damage in Cementitious Structures," Department of Civil & Environmental Engineering, University of Michigan,.
- [12] "Electrical Resistance Tomography for Subsurface Imaging," U.S. Department of Energy, Office of Environmental Management, Office of Science and Technology, 2000.
- [13] Priya M. Chimurkar, Alice N. Cheeran Vidya Sarode, "ELECTRICAL IMPEDANCE TOMOGRAPHY (EIT) BASED MEDICAL IMAGING USING FINITE ELEMENT METHOD (FEM) ," Xavier Institute of Engineering, Mumbai, India, 2012.
- [14] Gary Onik, Boris Rubinsky David M. Otten, "Distributed Network Imaging and Electrical Impedance Tomography of Minimally Invasive Surgery," University of California at Berkeley & Celebration Health Center for Surgical, 2004.
- [15] D. S. Holder, "Electrical Impedance Tomography of brain function," Departments of

Electronic Instrumentation for a 3D EIT Application

Medical Physics, University College London and Clinical Neurophysiology, University College Hospital, London, UK,.

- [16] R.Prabu, S.Raghavan R.Harikumar, "Electrical Impedance Tomography (EIT) and Its Medical Applications: A Review," *International Journal of Soft Computing and Engineering (IJSCE)*, 2013.
- [17] Jaako Malmivuo and Robert Plonsey, "26- Impedance Tomography," in *Bioelectromagnetism, Principles and Applications of Bioelectric and Biomagnetic Fields.*, 1995.
- [18] P. Kauppinen, J. Hyttinen, J. Malmivuo, "Sensitivity Distribution Simulations of Impedance Tomography Electrode Combinations ," Ragnar Granit Institute, Tampere University of Technology, Tampere, Finland, 2005.
- [19] Bentolhoda Ayati S., Kaddour Bouazza-Marouf, David Kerr, Michael O'Toole, "Performance evaluation of a digital electrical impedance tomography system.," Loughborough University & University of Manchester, *Imaging and Signal Processing in Health Care and Technology (ISPHT 2012)*, Baltimore, USA, 14-16, May 2012, pp.101-105..
- [20] D. Jennings, I. D. Schneider , "Front-end architecture for a multifrequency electrical impedance tomography system," *Medical and Biological Engineering and Computing* 2001, Volume 39, Issue 3, pp 368-374.
- [21] McEwan, G Cusick and D S Holder, "A Review of Errors in Multi-frequency EIT Instrumentation ," Department of Medical Physics and Bioengineering,UCL,London,.
- [22] Zurich Instruments AG, *HF2 User Manual.*, 2014.
- [23] LinkBone. <http://linkbone.com/>.
- [24] Universal Switching Corporation. <http://www.uswi.com/>.
- [25] National Instruments Corporation. www.ni.com/.
- [26] James Wei, "Using HF2IS Impedance Spectroscopy for FRA, 2-Terminal and 4-Terminal Measurements," Zurich Instruments AG, 2013.
- [27] Mari Lehti-Polojärvi, "Electrical Impedance Tomography applied to Stem Cells in Hydrogel Scaffold," Tampere University of Technology, 2014.
- [28] Analog Devices Corporation, "Fundamentals of Direct Digital Synthesis (DDS),".
- [29] Kevin R. Aroom, Matthew T. Harting, Charles S. Cox, Jr., Ravi S. Radharkrishnan, Carter Smith and Brijesh S. Gill, "Bioimpedance Analysis: A Guide to Simple Design and Implementation," 2008.

- [30] Mehran Zanganeh, "A new high output impedance wideband AC current source with high current swing authority for electrical impedance tomography applications," Department of Electrical Engineering, University of Guilan, Rasht, Iran., 2013.
- [31] David S Holder, *ELECTRICAL IMPEDANCE TOMOGRAPHY, Methods, History and Applications.*, 2005, pp. 84-120.
- [32] Yueh-Ching Teng and Kofi M. Odame, "A 10MHz 85dB Dynamic Range Instrumentation Amplifier for Electrical Impedance Tomography," Thayer School of Engineering, Dartmouth College, Hanover,.
- [33] Damian Martin Kirchmajer, Benedikt Steinhoff, Holly Warren, Ross Clark, Marc in het Panhuis, "Carbohydr. Res," in *Enhanced gelation properties of purified gellan gum.*, 2014, pp. 125–9.
- [34] Sung Chan Jun, Jihyeon Kuen, Jeehyun Lee, Eung Je Woo, David Holder and Jin Keun Seo, "Frequency-difference EIT (fdEIT) using weighted difference and equivalent homogeneous admittivity: validation by simulation and tank experiment," Department of Information and Communications, Gwangju Institute of Science and Technology, Korea, 2009.
- [35] M. I. N. Zhangl and I. H. M. Willison, "Electrical impedance analysis in plant tissues: The effect of freeze-thaw injury on the electrical properties of potato tuber and canot root tissues," Department of Biology, Dalhousie University, Halifax, Nova Scotia, Canada, 1991.

APPENDIX ATests on an R-C circuit (94 Ω at 100kHz) with the multiplexing system connected and without it.

FREQUENCY (Hz)	VALUE WITHOUT MUX SYSTEM		VALUE WITH MUX SYSTEM		ERROR OF THE MUX			
	Z (Ω)	Phi (Ω)	Z(Ω)	Phi (Ω)	ERROR Zmodule (Ω)	ERROR Zmodule (%)	ERROR PHI (Ω)	ERROR PHI (%)
1000.00	108.89	0.40	109.12	0.22	0.22	0.21	0.18	45.47
1268.96	109.11	0.24	109.18	0.08	0.07	0.06	0.15	64.60
1610.26	109.24	0.07	109.26	-0.03	0.02	0.02	0.10	144.26
2043.36	109.30	-0.08	109.30	-0.14	0.00	0.00	0.07	84.91
2592.94	109.32	-0.22	109.33	-0.26	0.02	0.01	0.05	21.30
3290.34	109.32	-0.36	109.34	-0.39	0.02	0.02	0.03	7.76
4175.32	109.31	-0.53	109.33	-0.54	0.02	0.02	0.01	2.01
5298.32	109.29	-0.72	109.30	-0.71	0.01	0.01	0.00	0.57
6723.36	109.25	-0.94	109.27	-0.93	0.02	0.02	0.01	1.11
8531.68	109.18	-1.22	109.19	-1.20	0.02	0.01	0.02	1.62
10826.37	109.05	-1.56	109.06	-1.54	0.01	0.01	0.03	1.81
13738.24	108.84	-1.99	108.86	-1.95	0.02	0.02	0.04	2.07
17433.29	108.50	-2.51	108.52	-2.45	0.02	0.01	0.05	2.17
22122.16	107.97	-3.13	107.98	-3.06	0.01	0.01	0.07	2.24
28072.16	107.16	-3.87	107.17	-3.78	0.01	0.01	0.09	2.34
35622.48	105.95	-4.68	105.96	-4.57	0.01	0.01	0.12	2.47
45203.54	104.22	-5.52	104.22	-5.38	0.00	0.00	0.15	2.65
57361.53	101.89	-6.27	101.88	-6.08	0.01	0.01	0.18	2.93
72789.54	99.06	-6.68	99.00	-6.44	0.06	0.06	0.25	3.68
92367.09	96.21	-6.81	96.16	-6.46	0.05	0.06	0.35	5.09
117210.23	93.05	-6.50	93.02	-6.08	0.03	0.03	0.43	6.55
148735.21	90.19	-5.64	90.16	-5.10	0.03	0.03	0.53	9.46
188739.18	87.88	-4.35	87.85	-3.68	0.03	0.03	0.68	15.53
239502.66	86.16	-2.79	86.14	-1.93	0.02	0.02	0.86	30.80
303919.54	84.96	-1.07	84.95	0.03	0.01	0.02	1.10	102.53
385662.04	84.16	0.78	84.16	2.17	0.00	0.00	1.40	179.70
489390.09	83.63	2.76	83.64	4.55	0.02	0.02	1.79	64.77
621016.94	83.27	4.94	83.31	7.23	0.05	0.06	2.29	46.31
788046.28	82.99	7.42	83.09	10.36	0.10	0.12	2.94	39.62
1000000.00	82.72	10.34	82.92	14.15	0.20	0.24	3.81	36.87
				MAX	0.22	0.24	3.81	179.70

APPENDIX B

Tests on an R-C circuit (94 Ω at 100kHz) through two different channels of the multiplexing system (Channel 3 and channel 15).

FREQUENCY (Hz)	CHANNEL 3		CHANNEL 15		ERROR BETWEEN CHANNELS			
	Z (Ω)	PHI (Ω)	Z (Ω)	PHI (Ω)	ERROR Zmodule (Ω)	ERROR Zmodule (%)	ERROR PHI (Ω)	ERROR PHI (%)
1000.00	109.39	0.06	109.29	0.05	0.10	0.09	0.01	10.69
1268.96	109.48	0.01	109.42	0.02	0.06	0.06	-0.01	74.13
1610.26	109.53	-0.08	109.47	-0.06	0.06	0.06	-0.02	25.25
2043.36	109.52	-0.17	109.48	-0.16	0.04	0.04	0.00	2.26
2592.94	109.57	-0.27	109.50	-0.26	0.07	0.07	-0.01	2.90
3290.34	109.56	-0.38	109.51	-0.38	0.05	0.05	-0.01	1.55
4175.32	109.55	-0.52	109.49	-0.52	0.06	0.05	-0.01	1.21
5298.32	109.52	-0.69	109.48	-0.68	0.04	0.04	-0.01	1.25
6723.36	109.50	-0.90	109.45	-0.90	0.05	0.04	0.00	0.07
8531.68	109.44	-1.17	109.38	-1.17	0.06	0.06	0.00	0.07
10826.37	109.32	-1.49	109.27	-1.50	0.05	0.05	0.00	0.17
13738.24	109.12	-1.90	109.07	-1.91	0.05	0.05	0.01	0.44
17433.29	108.79	-2.41	108.74	-2.40	0.05	0.05	0.00	0.16
22122.16	108.29	-3.01	108.24	-3.01	0.04	0.04	0.01	0.20
28072.16	107.50	-3.71	107.46	-3.72	0.04	0.04	0.01	0.31
35622.48	106.34	-4.49	106.31	-4.50	0.04	0.04	0.01	0.23
45203.54	104.70	-5.29	104.66	-5.31	0.04	0.04	0.02	0.30
57361.53	102.57	-6.03	102.52	-6.05	0.05	0.05	0.02	0.27
72789.54	99.85	-6.71	99.80	-6.74	0.04	0.04	0.02	0.37
92367.09	96.19	-6.76	96.14	-6.79	0.04	0.05	0.03	0.38
117210.23	93.11	-6.14	93.04	-6.18	0.07	0.08	0.03	0.55
148735.21	90.37	-5.14	90.30	-5.17	0.07	0.08	0.04	0.76
188739.18	88.11	-3.73	88.05	-3.78	0.06	0.07	0.05	1.28
239502.66	86.41	-2.01	86.34	-2.06	0.07	0.08	0.05	2.56
303919.54	85.22	-0.07	85.16	-0.14	0.06	0.08	0.07	94.43
385662.04	84.45	2.05	84.39	1.96	0.06	0.07	0.09	4.26
489390.09	83.97	4.39	83.91	4.28	0.06	0.07	0.11	2.44
621016.94	83.69	7.01	83.63	6.88	0.06	0.07	0.14	1.96
788046.28	83.53	10.09	83.48	9.92	0.05	0.06	0.18	1.76
1000000.00	83.48	13.79	83.42	13.55	0.05	0.06	0.24	1.74
					0.10	0.09	0.24	94.43

APPENDIX C

LabView program for impedance spectroscopy and real time impedance measurement. Provided by Zurich Instruments AG, Switzerland with slight modifications.

